Production of Highly Monodisperse Polystyrene by Evaporative Purification

by

Shipei Zhu

A thesis
presented to the University of Waterloo
in fulfillment of the
thesis requirement for the degree of
Master of Science
in
Physics (Nanotechnology)

Waterloo, Ontario, Canada, 2017

AUTHOR'S DECLARATION

I hereby declare that I am the sole author of this thesis. This is a true copy of the thesis, including any required final revisions, as accepted by my examiners.

I understand that my thesis may be made electronically available to the public.

Abstract

In this thesis, I will demonstrate a simple evaporative purification method to separate a polydisperse polystyrene with small molecular weight into highly monodisperse components (*N*-mers) ranging from 3-mers to 13-mers. This method has been applied to polystyrene samples of $\overline{M_w} = 600\ g/mol$ and $\overline{M_w} = 890\ g/mol$ with narrow molecular weight distribution, as well as a polystyrene sample of $\overline{M_w} = 1200\ g/mol$ with broader molecular weight distribution. In each case, the samples were successfully separated into milligram (mg) quantities of *N*-mers with *N* ranging from 3 to 13. The vapor pressure of each *N*-mer is calculated by using a simple lattice model and calculations suggest the isolated components have $\overline{M_w}/\overline{M_n}$ values less than 1.001 and, through a second iteration of the process, $\overline{M_w}/\overline{M_n}$ could become as low as 1.000003. The glass transition temperature (T_g) of each separated component is characterized by the differential scanning calorimeter and the T_g values of these components are independent of the sample they originate from. Based on the T_g values of these pure components, the Fox equation for the T_g of mixtures is developed into a simple relation which is able to accurately quantify the T_g values from oligomer to polymer.

Acknowledgements

Firstly, I would like to express my deep sense of gratitude and proud respect to my supervisor Dr. James Forrest who has guided and encouraged me at all stages of my project with great patience and immense care in the past two years. I am inspired by his persistent passion, extraordinary knowledge and perspective thoughts for science. Jamie is the best supervisor I have met!

I would also like to thank my other committee members: Mark Matsen and Kevin Musselman for their precious comments and selfless help during my master studies. I would also like to thank my GSP member professor Michel Gingras for his examination of my thesis defense. I would like to express the special thanks to Anja Drygala, Judy McDonnell, Lisa Pokrajac and Bonnie Findlay for their massive and necessary administrative work.

I would like to especially express my deep thanks to Yu Chai who is more than my fellow student. It is a wonderful experience to collaborate with Yu. Yu is more like my older brother who supports me in my studies and personal life. Any achievement of mine will not be possible without him. I highly appreciate valuable discussions from my other fellow students Fan-Yen Lin, Neha Dhalwani, Adam Raegen, Junjie Yin and Denzil Barkley. I am also grateful to have friends Yaowen Mei, Wei Cui and Wei Hong during my studies in University of Waterloo.

Finally, I am grateful to the endless love from my parents Fengyong Zhu and Qin Fang. I would also like to thank my older brother Shirui Zhu and my sister in law Na Dong for their continuous support in my life.

Table of Contents

AUTHOR'S DECLARATION ..... **ii**

Abstract ..... **iii**

Acknowledgements ..... **iv**

Table of Contents ..... **v**

List of Figures ..... **vii**

1. Introduction **1**

1.1 Introduction 1

1.2 Introduction to polydispersity index of polymers 1

1.3 Technologies for purification of polymers 5

1.3.1 Fractional distillation 6

1.3.2 Chromatographic fractionation 8

1.4 Lattice-Fluid theory of pure polymer melts 14

1.5 Introduction to the glass transition of polymer 29

1.6 Conclusion 35

2. Experimental Techniques **36**

2.1 Introduction 36

2.2 Sample Preparation 36

2.3 Vacuum system of thermal evaporation 37

2.4 Differential scanning calorimeter (DSC) 39

2.5 Conclusion 42

3. Numerical simulations of polystyrene purification by evaporation **43**

3.1 Introduction 43

3.2 Vapor pressure of polystyrene as a function of molecular weight and temperature 44
3.3 Polydispersity index (PDI) of purified polystyrenes based on molar fractions and evaporation rates 47
3.4 Conclusion 56
4. Experimental studies of polystyrene purification by evaporation 57
4.1 Introduction 57
4.2 Evaporative purification of high quality polystyrene with $\overline{M_w} = 600\ g/mol$ and $\overline{M_w} = 890\ g/mol$ 57
4.3 Evaporative purification of industrial grade polystyrene with $\overline{M_w} = 1200\ g/mol$ 64
4.4 Discussion 66
4.4.1 T_g values of separated components 66
4.4.2 Quantification of T_g from oligomer to polymer 68
5. Concluding remarks and future work 72
Reference 74
Appendix: published papers 79

List of Figures

Figure 1.2.1: The formation of polystyrene. In the process of polymerization, the carbon-carbon π bond of the vinyl group in the styrene monomer is broken and a new carbon-carbon σ bond is formed, attaching to the carbon of another styrene monomer. Styrene monomers interconnect in this way to comprise more chemically stable polystyrene, since newly formed σ bonds are much stronger than π bonds that were broken. Figure from https://en.wikipedia.org /wiki/Polystyrene. 2

Figure 1.2.2: Matrix-assisted laser desorption/ionization-time of flight (MALDI-TOF) spectrum of α,α'-bis-allyloxy functionalized polystyrene (the sample used was from the first fraction of the kinetic run). The peak difference is characterized as 104.2581 g/mol, which equals to the molecular weight of styrene monomer. The polystyrene sample with $\overline{M_n} = 2400\ g/mol$ and $\overline{M_w}/\overline{M_n} = 1.04$ still contains 19 different *N*-mer components with a Gaussian distribution of molar number intensity, as illustrated from 19 peaks of intensity. Figure from Ref. [6]. 4

Figure 1.3.1: Fractional distillation of crude oil. The fractionating column is hot at the bottom and cooler at the top. The difference in the temperature up and down the column separates different oil fractions. Larger molecules with high boiling point turn back into liquid at lower level, and smaller molecules with low boiling point rise up and condense at higher level. Figure from: *Science-resources.co.uk*. 6

Figure 1.3.2: Gel permeation chromatograms (GPC) of oligostyrene: I, II, original samples; II-a, II-b distilled fractions of sample II; I-a, I-b, I-c, I-d, resolved fractions of sample I by GPC; I-e, I-f, mixtures of sample I. The

repeating number of the main chain segments is indicated by a numeral. Number intensity of the sample was calculated by a Curve Resolver (du Pont Model 310) from the area of the resolved peaks. Separation in GPC occurs via porous beads (stationary phase) packed in column. Smaller molecules can enter pores more easily and spend more time in the column. Therefore, smaller molecules will elute last with larger elusion volume as indicated in figure. Figure from Ref. [9]. 9

Figure 1.3.3: Liquid chromatogram of polystyrene. Number intensity of each eluted sample is denoted by UV detector response. The detector is an LDC III differential UV detector operated at 254 nm wavelength. In LC, smaller molecules will flow out the column earlier due to weaker sorption with the stationary phase. Digital number on each resolved peak denotes the molecular weight of each eluted sample. Figure from Ref. [18]. 10

Figure 1.3.4: Mass spectra of polystyrene. (a) In EI (70 eV) spectrum, a strong base peak at 91 g/mol indicated ion ($C_7H_7^+$) was observed. No ions above 682 g/mol were observed. (b) In FD (16 mA) spectrum, ions with molecular weight from 474 g/mol to 1930 g/mol were observed, and neighboring ions were separated by 104 g/mol unit. Figure from Ref. [18]. 11

Figure 1.3.5: A typical SFC-ELSD chromatogram for fractionation of PEG with $\overline{M_w} = 1000\ g/mol$ at an injected concentration of 100 mg/mL. The injection volume was 5 μL. The darker background shows the fractionation time area and lighter background shows the discard time area. Figure from Ref. [19]. 13

Figure 1.4.1: A lattice mixture of N_0 holes (denoted as yellow spheres) and N_1 pure polymer molecules (denoted as chains with connected brown spheres).

Each pure polymer molecule occupies r lattice sites (r =8 in this figure). The total number of lattice sites is $N_r = N_0 + rN_1$. Figure from Ref. [24]. 15

Figure 1.4.2: Reduced pressure-temperature diagrams for $r = 1$. Any $(\tilde{P}, \tilde{T})$ point inside the metastable region yields a free energy diagram with two minima similar to Fig. 1.4.4. Any $(\tilde{P}, \tilde{T})$ point on the coexistence line yields a free energy diagram with two equal minima similar to Fig.1.4.7. Any $(\tilde{P}, \tilde{T})$ point outside the metastable region yields a free energy diagram with a single minima. 23

Figure 1.4.3: Schematic representation of the solutions of the equation of state (Eq.1.4.27). Values of parameters used in this calculation are: $r = 1, \tilde{P} = 0.02, \tilde{T} = 0.35$. Curves are plotted based on Eq.1.4.28. Solutions at the lowest and highest values of $\tilde{\rho}$ correspond to minima in $\tilde{G}$; the intermediate solution corresponds to a maximum in $\tilde{G}$. See Fig.1.4.4. 24

Figure 1.4.4: Reduced Gibbs free energy vs reduced density at a pressure and temperature where liquid-like phase is metastable with respect to the vapor-like phase. This curve is plotted based on Eq. (1.4.20) and parameters used in this calculation are the same as those used in Fig.1.4.3. 25

Figure 1.4.5: Schematic representation of the solutions of the equation of state (Eq.1.4.27). Values of parameters used in this calculation are: $r = 1, \tilde{T} = 0.45$. Curves are plotted based on Eq.1.4.28 and Eq.1.4.34. The solution at the lower $\tilde{\rho}$ correspond to minima in $\tilde{G}$; the solution at the higher $\tilde{\rho}$ corresponds to an inflexion point in $\tilde{G}$ curve. See Fig.1.4.6.....26

Figure 1.4.6: Reduced Gibbs free energy vs reduced density when $(\tilde{P}, \tilde{T})$ point is on the “stability limit for liquid” boundary of the “metastable” region. This

curve is plotted based on Eq. (1.4.20) and parameters used in this calculation are the same as those used in Fig.1.4.5.....27
Figure 1.4.7: Binodal condition when Gibbs free energy values for the vapor-like phase and the liquid-like phase are equal. 28
Figure 1.5.1: Temperature dependence of a liquid's volume or enthalpy at constant pressure. The liquid-equilibrium state is denoted as the white straight line. The transition curve of crystallization is denoted as the blue polyline. T_m is the melting temperature. A slow cooling rate produces a glass transition at T_{ga}; a faster cooling rate leads to a glass transition at T_{gb}. Figure from Ref. [33]. 31
Figure 2.3.1: Top view of thermal vacuum apparatus (left); side view of the thermal vacuum apparatus (right). The apparatus consists of vacuum pump, spacers, removable collector, and Linkam heating stage integrated with proportional-integral-derivative temperature controller. 38
Figure 2.4.1: Schematic of the interior of a DSC. Thermoelectric disc as temperature controller is powered by cylindrical furnace. Thermocouple sensor below reference/sample pan monitors temperature of that pan. The DSC ultimately outputs the differential heat flow between material and the empty reference pan. Figure from *Operation Manual of TA Instruments Q100 DSC*.....40
Figure 2.4.2: Determination of T_g from DSC curve. T_g measurement of $\overline{M_w} = 600\ g/mol$ polystyrene with $\overline{M_w}/\overline{M_n}$ =1.2 by Q100 DSC operated at 10 ℃/min cooling rate. The inflexion point of the function curve is associated with T_g value and it is calculated by Analysis Software of Universal V4.7A TA Instruments via the first derivative of the glass

transition curve. For this data, T_g is -9.28 ℃, which locates at the midpoint of the incline. 41
Figure 3.2.1: Calculated vapor pressures for polystyrene *N*-mers as a function of temperature and polymerization index *N*. The reduced pressure $\tilde{P}$ and temperature $\tilde{T}$ have been converted to real physical values. 45
Figure 3.3.1: The mole number of *N*-mer polystyrene in mixture as a function of evaporation time at temperature 270 ℃ for *N*=8~11, which is calculated from Eq. (3.3.10). "α-Evaporation Time" denotes that the real time scale of evaporation is determined by the constant α, which will be further determined by experiment. The value of α is set as 10^4 for simplicity of the simulation. 51
Figure 3.3.2: The mole number of *N*-mer polystyrene in mixture as a function of evaporation time at temperature 290 ℃ for *N*=9~11, which is calculated from Eq. (3.3.10). "α-Evaporation Time" denotes that the real time scale of evaporation is determined by the constant α, which will be further determined by experiment. The value of α is set as 10^4 for simplicity of the simulation. 52
Figure 3.3.3: Initial molecular weight distribution of polystyrene mixture, and products after simulated evaporative purification method described in the text. Mole numbers of initial *N*-mer polystyrenes are set as $n_1 = n_{11} = 4.6\,mol$, $n_2 = n_{10} = 6.5\,mol$, $n_3 = n_9 = 8.3\,mol$, $n_4 = n_8 = 9.25\,mol$, $n_5 = n_7 = 9.8\,mol$, $n_6 = 10\,mol$, with mole number fractions following Gaussian distribution. 53

Figure 3.3.4: The relevant "$\overline{M_w}/\overline{M_n}$" of each separated polystyrene product calculated in Fig. 3.3.3.....54
Figure 3.3.5: "$\overline{M_w}/\overline{M_n}$ -1" as a function of iteration times at 290 ℃. 55
Figure 4.2.1: Schematic diagram showing the procedure for evaporative deposition of polystyrenes. 58
Figure 4.2.3: Mass distributions of evaporated components during the process of evaporation. The masses evaporated from the $\overline{M_w} = 600\ g/mol$ PS are labelled by the blue star symbols, and the masses evaporated from the $\overline{M_w} = 890\ g/mol$ PS are labelled by the red open circles. The fitting curves are based on Gaussian functional forms and are simply meant to guide the eye. The blue fitting curve is for the $\overline{M_w} = 600\ g/mol$ PS; the red fitting curve is for the $\overline{M_w} = 890\ g/mol$ PS.....62
Figure 4.3.1: Measured deposited mass and T_g values of evaporatively isolated components of *N*-styrene for $\overline{M_w} = 1200\ g/mol$ polystyrene sample. The deposited mass of each 2 hours is labelled as red triangle symbol. T_g values of isolated *N*-styrene are labelled as blue square symbols. T_g values exhibiting plateaus are marked by green lines.....65
Figure 4.4.1: T_g values of *N*-styrene as isolated from the 3 different initial polydisperse polystyrenes, as well as the T_g values of the initial polydisperse samples. T_g values of $\overline{M_w} = 600\ g/mol$, $\overline{M_w} = 890\ g/mol$ and $\overline{M_w} = 1200\ g/mol$ initial polydisperse polystyrenes are labelled as green circle symbol, red square symbol and blue square symbol, respectively. T_g values of *N*-styrene isolated from $\overline{M_w} = 600\ g/mol$, $\overline{M_w} = 890\ g/mol$ and $\overline{M_w} = 1200\ g/mol$ polystyrenes are labelled as open triangle symbols, open circle

symbols and open square symbols, respectively. The polymerization index N of each isolated styrene is estimated by Fox-Flory relation as introduced in section 1.5. T_g values of isolated N-styrene are from T_g values exhibiting plateaus in Fig. 4.2.2 and Fig. 4.3.1.....67

Figure 4.4.2: T_g values of N-styrene ($N \leq 11$), and more polydisperse ($N > 11$) polystyrene and fits to Eq. (4.4.3) as well as Fox-Flory expressions. These N-styrenes are from the $\overline{M_w} = 890\ g/mol$ PS as described in this experiment; while these more polydisperse polystyrenes are the same type as the N-styrenes. 71

1. Introduction

1.1 Introduction

In this chapter, the relevant physics we need to consider for the work will be discussed. I will give an introduction to polydispersity index of polymers as well as existed technologies for purification of polymers. I will also introduce the Lattice-Fluid theory of pure polymer melts and how it can be used to calculate vapor pressures of pure polymers. Finally, I will discuss the glass transition of polymer and its relation with molecular weight of polymer.

1.2 Introduction to polydispersity index of polymers

Polymers, also known as macromolecules, are built up of a large number of molecular units that are linked together by covalent bonds [1]. Polymers are generally synthesized from monomers by a chemical process known as polymerization. Take polystyrene (PS), for example; styrene is the monomer, which combines together as repeat units to form PS, as shown in Fig.1.2.1. The number of repeat units determines the degree of polymerization denoted by N. A polymer sample is monodisperse if it is composed of all identical polymers with the same degree of polymerization N. Some naturally produced biopolymers, such as proteins, are found to be almost completely monodisperse. However, for the majority of polymer systems, it is impossible to produce real monodisperse

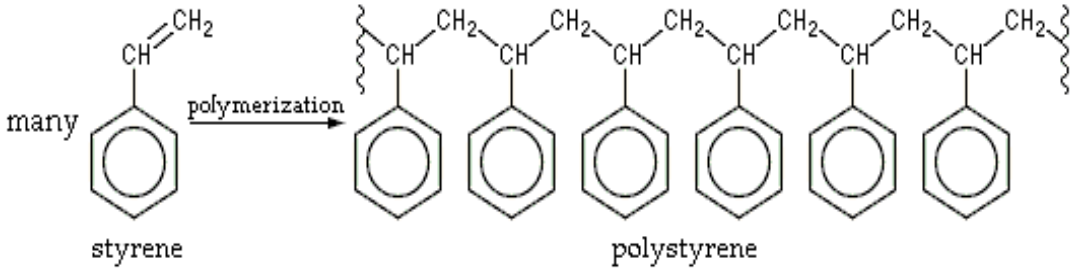

Figure 1.2.1: The formation of polystyrene. In the process of polymerization, the carbon-carbon π bond of the vinyl group in the styrene monomer is broken and a new carbon-carbon σ bond is formed, attaching to the carbon of another styrene monomer. Styrene monomers interconnect in this way to comprise more chemically stable polystyrene, since newly formed σ bonds are much stronger than π bonds that were broken. Figure from https://en.wikipedia.org/wiki/Polystyrene.

samples by common synthetic methods. The reason is that the incorporation of monomer units into polymer molecules as a polymerization reaction follows certain statistical principles, which leads to the product of such a reaction never being homogeneous at the molecular level [2]. For example, reactive centers in chain polymerizations are created at the beginning and become shifted to the new end of the chain after the reaction with monomers, and this process of reaction results in a mixture of macromolecules with a Poisson distribution of N [1]. Many different physical properties of polymers, such as the glass transition temperature (T_g) [3], solubility [4], and viscoelasticity [5], are strongly dependent on polymerization index N. Therefore, to study the molecular properties of polymer, one has to consider the related molecular weight distribution. The polydispersity index (PDI) is widely used to characterize the molecular weight

distribution of a polymer sample. The number-average molecular weight $\overline{M_n}$ is obtained by dividing the total molecular weight of all polymer chains in the sample into the total number of all polymer chains:

$$\overline{M_n} = \frac{\sum N_i M_i}{\sum N_i} \tag{1.2.1}$$

where M_i is the molecular weight of *i*-th polymer chain in the sample and N_i is the number of chains of that molecular weight. The weight-average molecular weight $\overline{M_w}$ is defined as:

$$\overline{M_w} = \frac{\sum N_i {M_i}^2}{\sum N_i M_i} . \tag{1.2.2}$$

The polydispersity index is the ratio of the weight-average molecular weight and the number-average molecular weight:

$$\text{PDI} = \frac{\overline{M_w}}{\overline{M_n}} . \tag{1.2.3}$$

Since $\overline{M_w}$ is larger than $\overline{M_n}$ for polymer mixture, $\text{PDI} > 1$ always exists in a real polymer sample and $\text{PDI} = 1$ is just for the theoretically monodisperse polymer. Higher PDI indicates wider molecular weight distribution. The best synthetic polymers with PDI ranging from 1.02 to 1.10 are considered to be very monodisperse. However, an illustrated example given by matrix-assisted laser desorption/ionization-time of flight (MALDI-TOF) spectrum mass analysis of

polystyrenes can show how misleading this criterion can be. As shown in Fig. 1.2.2, a PS sample with $\overline{M_n} = 2400\ g/mol$ and PDI $= 1.04$, which is usually described as a monodisperse sample, still contains 19 different *N*-mers.

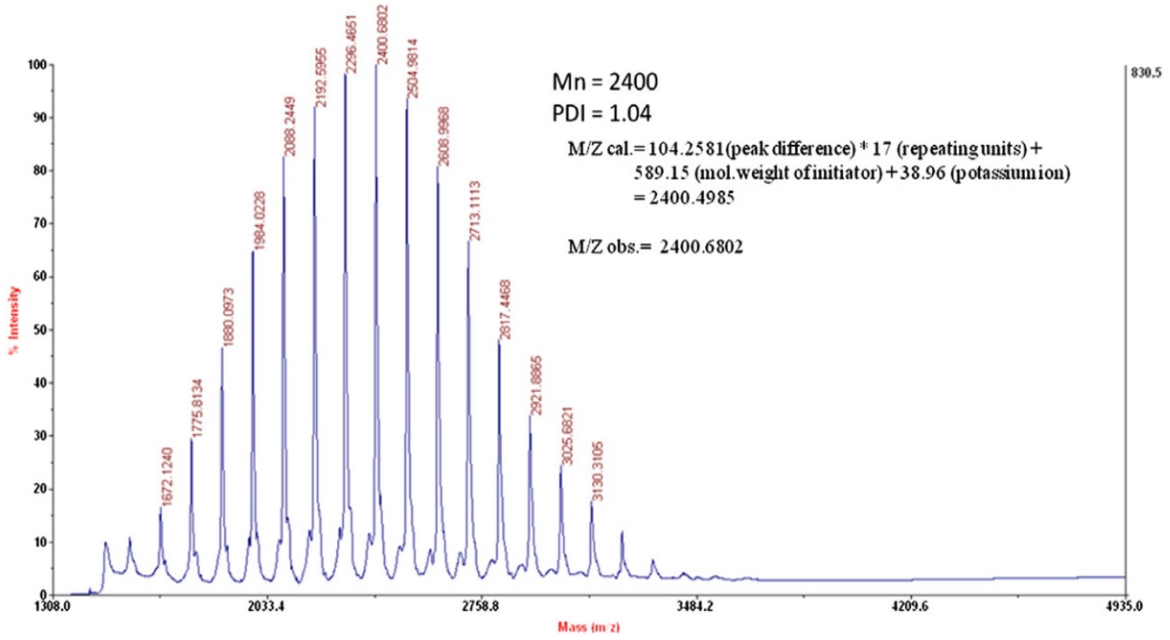

Figure 1.2.2: Matrix-assisted laser desorption/ionization-time of flight (MALDI-TOF) spectrum of α,α'-bis-allyloxy functionalized polystyrene (the sample used was from the first fraction of the kinetic run). The peak difference is characterized as 104.2581 g/mol, which equals to the molecular weight of styrene monomer. The polystyrene sample with $\overline{M_n} = 2400\ g/mol$ and $\frac{\overline{M_w}}{\overline{M_n}} = 1.04$ still contains 19 different *N*-mer components with a Gaussian distribution of molar number intensity, as illustrated from 19 peaks of intensity. Figure from Ref. [6].

The inherent distributions of molecular weight result in disperse structure-property relations, which limits the establishment of basic correlations between the chemical nature of polymer carriers and the resulting biological response [7].

Furthermore, the conjugated chain length is one of the major factors governing the electronic and optoelectronic properties of conjugated polymers and more monodisperse conjugated polymers could be used to significantly enhance the efficiencies of polymer light-emitting diodes and polymer solar cells [8]. The necessity of highly monodisperse polymers with no distribution in degree of polymerization is also widely recognized by polymer physicists [9-13] who aim to obtain precise measurements of physical properties of polymers or oligomers at a molecular weight of interest. Unfortunately, the completely monodisperse synthetic polymers have not been commercially available so far. The present best monodisperse synthetic polymers with $\mathrm{PDI} = 1.02$ are usually prepared by the living anionic polymerization [14,15], which requires complicated synthetic routes carried out by experienced chemists.

1.3 Technologies for purification of polymers

As mentioned in Section 1.2, none of the present established polymerization methodologies can produce monodisperse polymers with defined monomer sequences. Thus, numerous physically based technologies for purification of polymers have been developed to achieve the production of completely monodisperse polymers. Fractional distillation and chromatographic fractionation are two of these technologies and will be mainly introduced in this section.

1.3.1 Fractional distillation

Fractional distillation separates the compounds into its component parts by using the significant difference in boiling points of these components under atmospheric pressure. Thousands of years ago, people used this technology to distill fresh water from seawater [16]. Nowadays, this technology is well developed and is widely used in industry, especially for the refinery of petroleum.

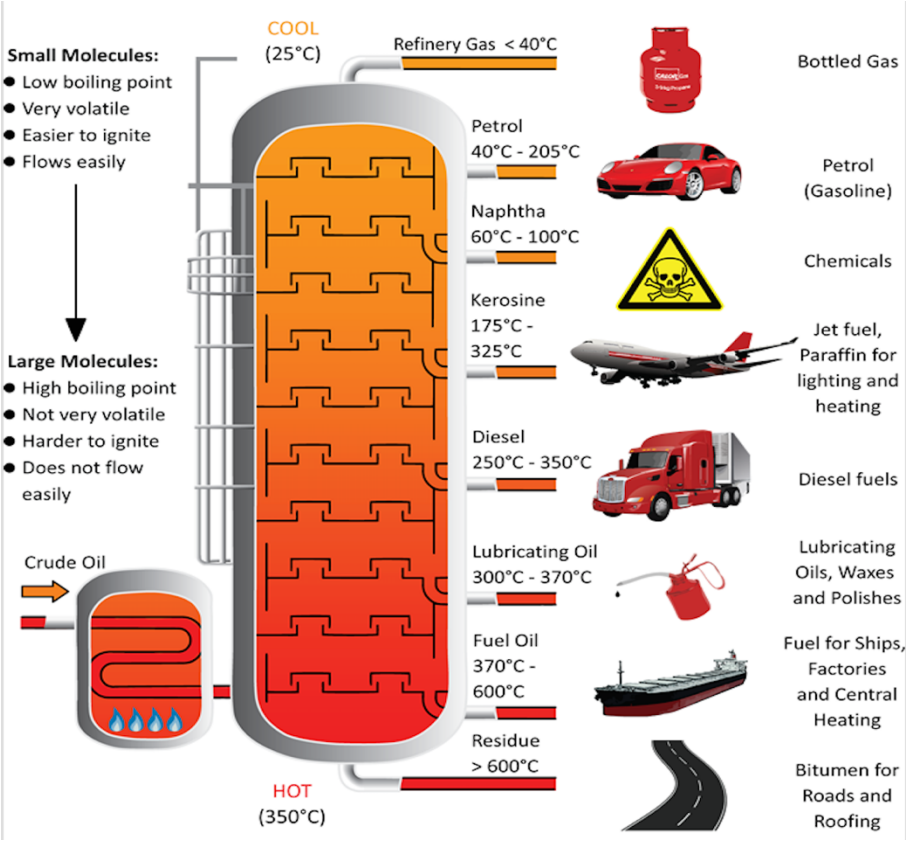

Figure 1.3.1: Fractional distillation of crude oil. The fractionating column is hot at the bottom and cooler at the top. The difference in the temperature up and down the column separates different oil fractions. Larger molecules with high boiling point turn back into liquid at lower level, and smaller molecules with low boiling point rise up and condense at higher level. Figure from: *Science-resources.co.uk*.

As illustrated by Fig.1.3.1, the bottom of the fractionating column where the gas of crude oil enters is hottest and the temperature of each tower layer becomes cooler with the increased height. The larger hydrocarbons with higher boiling points condense at lower levels, while the smaller hydrocarbons with lower boiling points remain as gas and will continue to rise up and condense at higher levels. As a result, different types of oil products are sorted at each layer of the column. However, it is notable that each product is still a mixture, for example fuel oil contains hydrocarbons with degree of polymerization ranging from 30 to 40. Fractional distillation is also quite applicable for the purification of volatile chemicals, such as ethanol, toluene and acetone, whose vapor pressures are close to atmospheric pressure. For chemicals with much lower vapor pressure, vacuum technology is usually introduced in the distillation. For polymers, vacuum distillation has been mainly utilized for the fractionation of monomers, dimers and trimers. For instance, Tatsuko and Mitsuru proposed the fractionation of dimers and trimers of oligostyrene by vacuum distillation [9]. They prepared two types of styrene oligomers (sample I and II) with different end groups. The fractions of sample II obtained by vacuum distillation were characterized by gel permeation chromatograms (GPC) and the resulting signals of chromatograms are shown as II-a and II-b in the left hand part of Fig.1.3.2. Based on the peaks

of signals, the dimer-rich fraction II-a still contains an appreciable amount of trimers, while trimer-rich fraction II-b contains a non-negligible amount of dimers. It is obvious that fractional distillation alone is not enough to separate pure components. Thus, Tatsuko and Mitsuru further separated the distilled fractions by GPC to obtain purer samples.

1.3.2 Chromatographic fractionation

While fractional distillation is usually applied for the fractionation of dimers and trimers, chromatographic fractionation is a preferred choice to separate N-mers with higher degree of polymerization. Chromatographic fractionation is based on the fact that a dynamic equilibrium is established between the concentration of a solute in the mobile phase and the stationary phase [17]. The mobile phase is a fluid which can be either a liquid or a gas, while the stationary phase usually appears to be a solid consisting of fine particles or porous beads packed in a column [17]. The flow rate of each solute molecule in the chromatography depends on attractions of the two phases, and molecules having higher attractions will move more quickly. Chromatographic fractionation separates components by utilizing their different flow rates. This section will introduce the purification work of N-mers carried out by 3 types of chromatography: gel permeation

chromatograms (GPC), liquid chromatography (LC) and supercritical fluid chromatography (SFC).

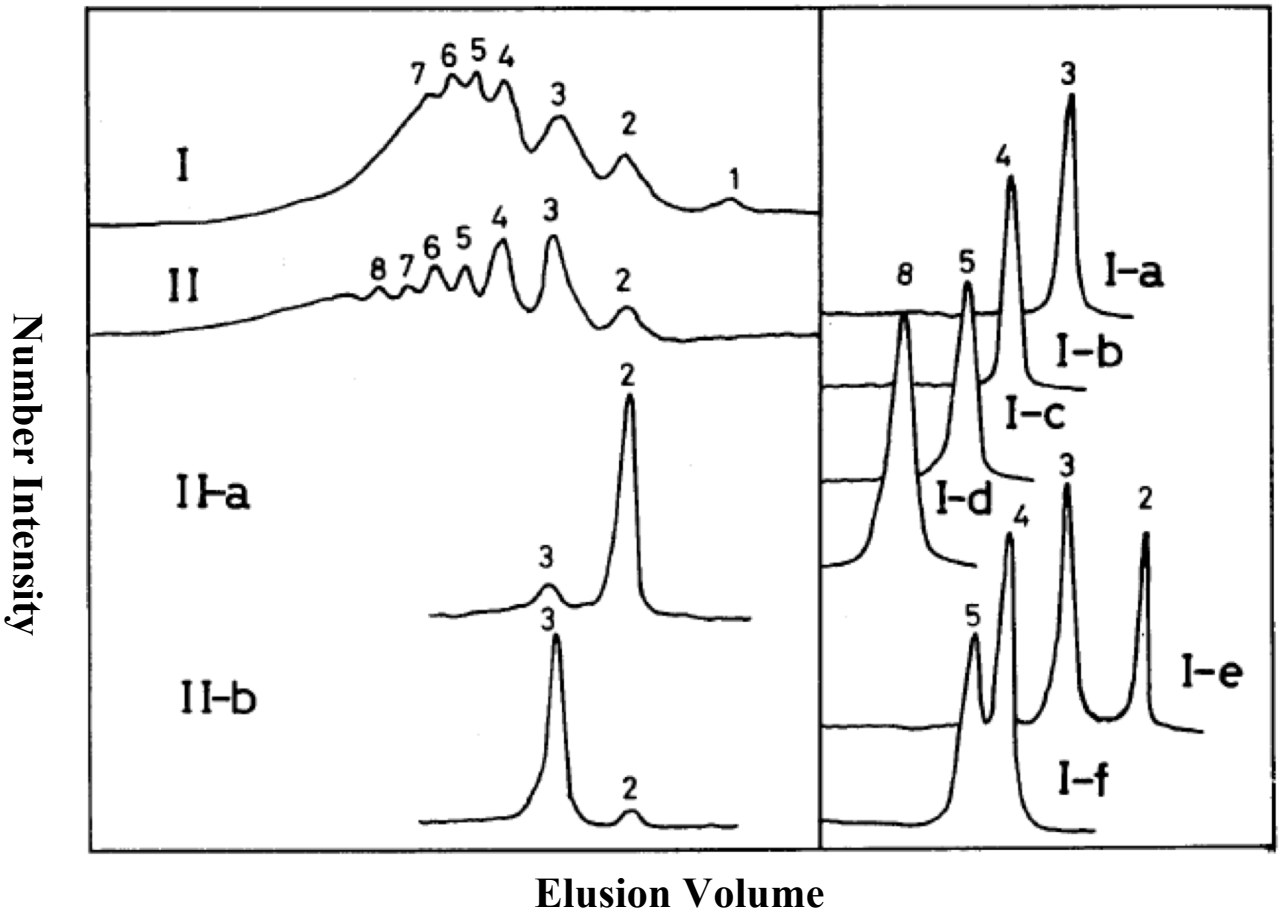

Figure 1.3.2: Gel permeation chromatograms (GPC) of oligostyrene: I, II, original samples; II-a, II-b distilled fractions of sample II; I-a, I-b, I-c, I-d, resolved fractions of sample I by GPC; I-e, I-f, mixtures of sample I. The repeating number of the main chain segments is indicated by a numeral. Number intensity of the sample was calculated by a Curve Resolver (du Pont Model 310) from the area of the resolved peaks. Separation in GPC occurs via porous beads (stationary phase) packed in column. Smaller molecules can enter pores more easily and spend more time in the column. Therefore, smaller molecules will elute last with larger elusion volume as indicated in figure. Figure from Ref. [9].

As mentioned in Section 1.3.1, GPC is used to separate the oligostyrene into pure N-mer styrenes. As shown in the right hand part of Fig.1.3.2, the peaks are distinguished up to 8-mer and higher molecular weight N-mers than 8-mer are difficult to be precisely detected by GPC, since the resolution factor of the column decreases with the increasing molecular weight [9].

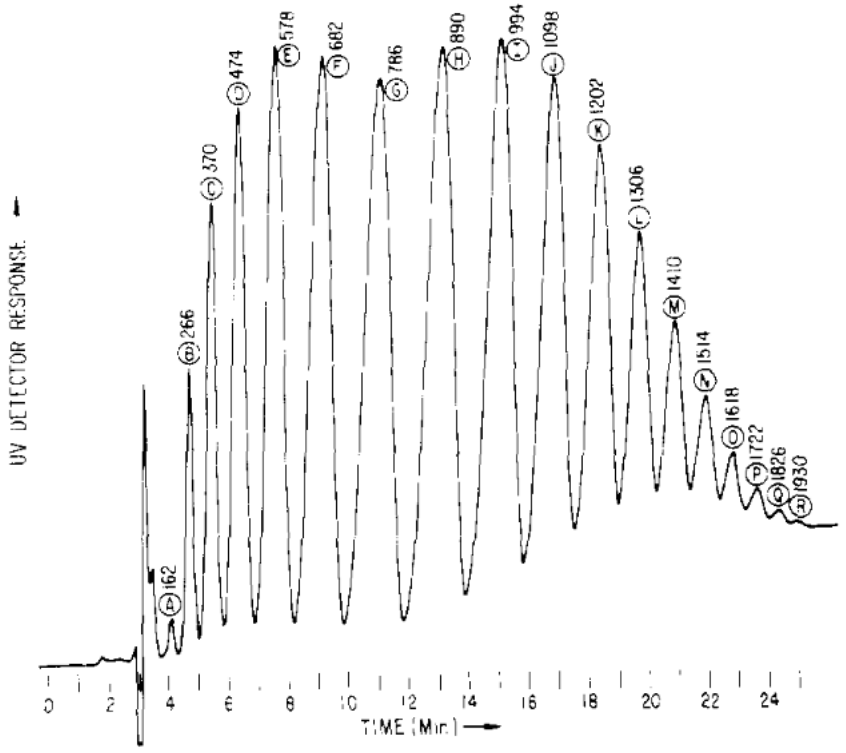

Figure 1.3.3: Liquid chromatogram of polystyrene. Number intensity of each eluted sample is denoted by UV detector response. The detector is an LDC III differential UV detector operated at 254 nm wavelength. In LC, smaller molecules will flow out the column earlier due to weaker sorption with the stationary phase. Digital number on each resolved peak denotes the molecular weight of each eluted sample. Figure from Ref. [18].

Oligomers containing up to 18 monomer units were separated and identified from the polystyrene samples of reported $\bar{M}_n = 750\ g/mol$ via liquid chromatograp-

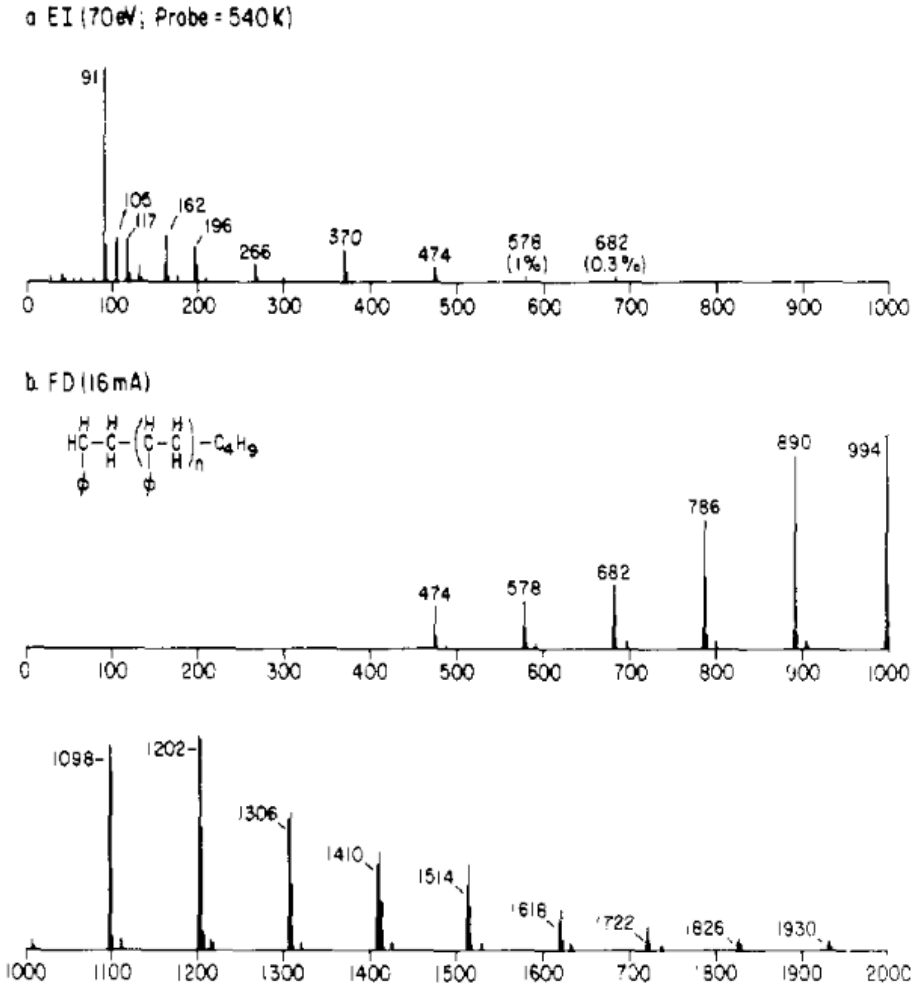

Figure 1.3.4: Mass spectra of polystyrene. (a) In EI (70 eV) spectrum, a strong base peak at 91 g/mol indicated ion ($C_7H_7^+$) was observed. No ions above 682 g/mol were observed. (b) In FD (16 mA) spectrum, ions with molecular weight from 474 g/mol to 1930 g/mol were observed, and neighboring ions were separated by 104 g/mol unit. Figure from Ref. [18].

hy-field desorption mass spectroscropy which was well developed by Robert *et al*. [18]. This liquid chromatograph (LC) was equipped with a Water μBondapak C_{18} column, with the size of 30 $cm\times$3.9 mm. As shown in Fig.1.3.3, a single 0.73 mg polystyrene sample was separated into N-mer oligomeric styrenes. The molecular weight of obtained N-mers were then directly analyzed by coupled electron impact (EI) and field desorption (FD) mass spectra, as shown in Fig. 1.3.4. The EI spectrum only detected the N-mers with molecular weight up to 682 g/mol. While higher molecular weight N-mers were observed by the FD spectra, monomers, dimers and trimers were not observed due to evaporation at the heating current of 16 mA. All the N-mers with a wide range of molecular weight from 105 g/mol to 1930 g/mol can be detected by the two complementary spectrums. The oligomers were separated by the units of 104 g/mol associated with the styrene monomer unit. Based on the molecular weights determined by the FD spectrum and the peak heights of the LC chromatogram, the number average molecular weight was calculated to be 853 g/mol, which indicated that the coupled LC-FD spectrum can not only separate pure N-mers, but also improves the resolution of the characterization.

It is more difficult for chromatography to separate N-mers of polyethylene glycol (PEG), since the molecular weight of its repeating unit is only 44 g/mol, which

is much smaller than that of polystyrene (104 g/mol). Recently, Kayori *et al.* [19] reported a molecularly uniform PEG that was separated from the PEG sample with average molecular weight 1000 g/mol by supercritical fluid chromatography (SFC). An SFCpak SIL-5 silica gel column with a pore size of 6 nm and a particle size of 5 μm was employed in the SFC, which had a more refined structure in comparison with the above column designed for the polystyrene. A PEG sample with an injection volume of 5 μL was fractionated

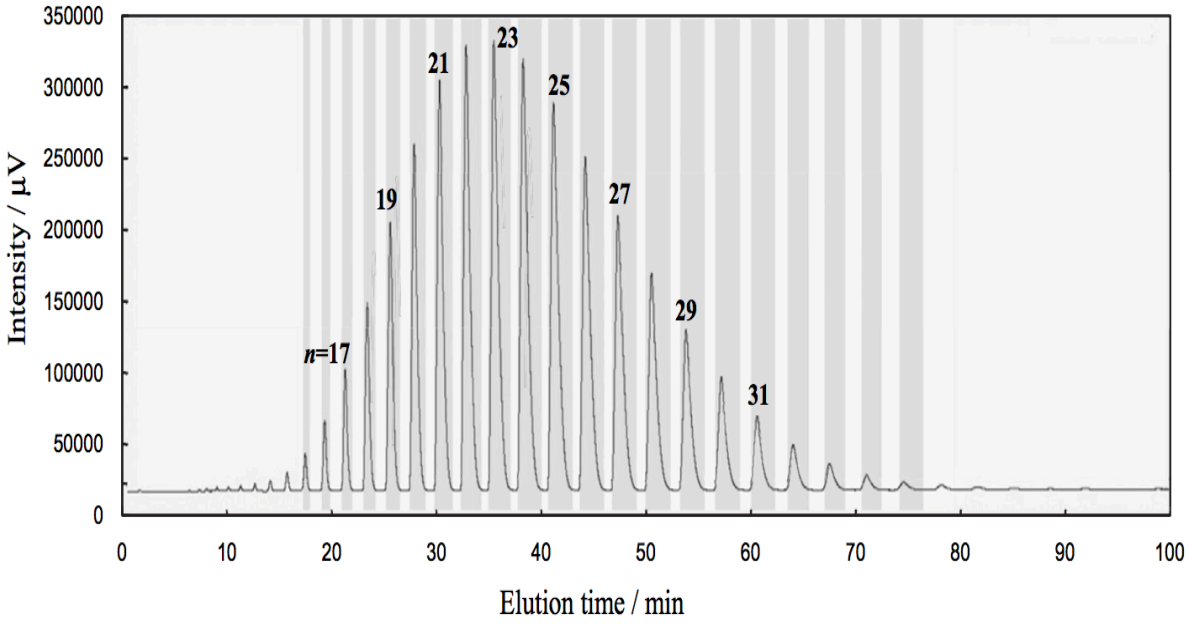

Figure 1.3.5: A typical SFC-ELSD chromatogram for fractionation of PEG with $\overline{M_w}$=1000 g/mol at an injected concentration of 100 mg/mL. The injection volume was 5 μL. The darker background shows the fractionation time area and lighter background shows the discard time area. Figure from Ref. [19].

by the SFC and the obtained fractions were detected by evaporative light-scattering detector (ELSD). As shown in Fig.1.3.5, all the components of the PEG

sample were completely isolated. The 23-mer rich product was then analyzed by matrix-assised laser desorption/ionization time-of-flight mass spectrometer (MALDI- TOF-MS) and the result of analysis demonstrated that this product contained 23-mer with the mass fraction of more than 98.5%.

In conclusion, GPC, LC and SFC with special designs are reported to have an excellent ability to separate highly monodisperse oligomers. However, the largest quantity of fractions purified by the chromatographic fractionation is still limited at the milligram level. In contrast, fractional distillation is able to purify vast amount of water, low molecular weight hydrocarbons and volatile chemicals whose vapor pressures are approaching atmospheric pressure. For polymers whose vapor pressures are not that large, vacuum techniques are usually employed in fractional distillation. Vacuum distillation is currently only applied for dimers and trimers. In fact, some polymers with an extended range of N, such as aliphatic chain molecules [20], still have non-negligible vapor pressure. Vacuum distillation remains to be explored for larger molecular weight polymers.

1.4 Lattice-Fluid theory of pure polymer melts

Vacuum distillation separates the single component from the mixture via the significant difference in the vapor pressures of these components. In order to demonstrate the feasibility of the vacuum distillation for polymers with an

extended range of N, the vapor pressure of each N-mer should be investigated. The vapor pressures of some polymer solutions, such as polystyrene solutions in toluene and methyl ethyl ketone [21] and poly(vinyl Alcohol) solutions in water [22], have been measured. However, there are few measurements of any pure polymers (not in solution), and certainly none of pure N-mer systems of polystyrene. Fortunately, the Lattice-Fluid theory of pure polymer melts described by Sanchez *et al.* [23] is found to be a useful theory for the prediction of vapor pressure of each N-mer.

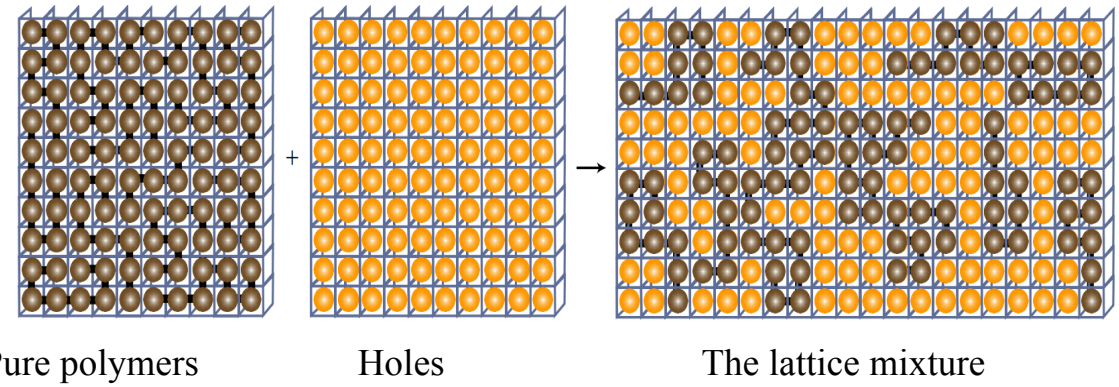

Figure 1.4.1: A lattice mixture of N_0 holes (denoted as yellow spheres) and N_1 pure polymer molecules (denoted as chains with connected brown spheres). Each pure polymer molecule occupies r lattice sites (r =8 in this figure). The total number of lattice sites is $N_r = N_0 + rN_1$. Figure from Ref. [24].

The Lattice-Fluid theory of pure polymer melts is quite similar to the Flory-Huggins solution theory [25]. This lattice model contains a mixture of pure polymers and vacant lattice sites (holes) rather than the solvent molecules in the lattice

system of Flory-Huggins solution theory [25], as shown in Fig.1.4.1. Each hole is taken to occupy a single lattice site. It is notable that each monomer has a chosen shape and size and therefore each monomer can occupy more than one lattice sites [26]. A polymer chain with polymerization index N can then be considered to occupy r lattice sites. N and r are not the same and are related by:

$$r = c_0 N \qquad (c_0 \geq 1)\,, \tag{1.4.1}$$

where c_0 is the number of lattice sites occupied by each monomer and the determination of c_0 will be later introduced in this section. The most difficult problem for obtaining the Gibbs free energy of this system is to determine the number of possible configurations. At this point, Sanchez employed the Guggenheim solution [27-29] for a binary mixture of pure polymer molecules and holes to obtain an approximate configuration number.

To discuss the derivation of the Guggenheim solution, several notations [23] need to be introduced:

(1) The total number of lattice sites of this binary system which contains N_1 N-mers (each N-mer occupies r lattice sites) and N_0 holes is:

$$N_r = N_0 + rN_1. \tag{1.4.2}$$

(2) If the coordination number of the lattice considered is z, each lattice site of the middle chain will be surrounded by $(z-2)$ nearest non-bonded neighbors

and 2 bonded neighbors, while the chain ends will have one bonded neighbor and $(z-1)$ non-bonded neighbors. As a result, each N-mer will have qz non-bonded neighbors where

$$qz = (r-2)(z-2) + 2(z-1) = r(z-2) + 2. \quad (1.4.3)$$

(3) The total number of nearest neighbor pairs in the system is $(z/2)N_r$, among which $(z/2)N_q$ is the number of the non-bonded pairs where

$$N_q = N_0 + qN_1. \quad (1.4.4)$$

The relation of the numbers N_r, N_0, N_q and N_1 satisfies:

$$(z/2)N_q = (z/2-1)N_r + N_1 + N_0. \quad (1.4.5)$$

(4) One of parameters characterizing a N-mer is the symmetry number σ. For a linear N-mer with indistinguishable chain ends, σ is equal to 2. For a linear N-mer with distinguishable chain ends, σ is equal to 1.

(5) The flexibility parameter δ is another important parameter to characterize a N-mer by measuring the internal degrees of freedom of the N-mer. It is the number of ways of arranging the N-mer on the lattice after one lattice site has been occupied by the polymer chain. For $r = 1$, $\delta = 1$; for $r = 2$, $\delta = z$. For a flexible polymer chain with $r = 3$, $\delta = z(z-1)$. For a long and flexible N-mer occupying r lattice sites, the maximum value of δ is:

$$\delta_{max} = z(z-1)^{r-2}. \tag{1.4.6}$$

Based on Guggenheim solution, the number of configurations available to this system is [27-29]:

$$\Omega = \left(\frac{\delta}{\sigma}\right)^{N_1} \frac{N_r!}{N_0!\,N_1!}\left(\frac{N_q!}{N_r!}\right)^{z/2}, \tag{1.4.7}$$

which has the following limiting form for large z by using Sterling's approximation ($n! \cong (n/e)^n$) and Eq. (1.4.5):

$$\lim_{z\to\infty} \Omega = \left(\frac{1}{f_0}\right)^{N_0}\left(\frac{\omega}{f}\right)^{N_1}, \tag{1.4.8}$$

where $\omega = \delta r/\sigma e^{r-1}$, the empty sites fraction $f_0 = N_0/N_r$ and the fraction of occupied sites $f = rN_1/N_r$.

The following calculations will be based on Eq. (1.4.8). In addition, two assumptions are made by Sanchez *et al.* [23]:

(1) The flexibility parameter δ is independent of temperature and pressure.

(2) The close packed volume rv^* of a molecule is independent of temperature and pressure. The close packed volume of a mer is v^*, which is also the volume of a lattice site. The close packed volume of the N_1 N-mers (with each N-mer occupying r lattice sites) without holes is:

$$V^* = N_1(rv^*). \tag{1.4.9}$$

If the close packed mass density is set as ρ^*, then the close packed molecular volume can be expressed as:

$$rv^* = M/\rho^* = M_0 N/\rho^* \,, \tag{1.4.10}$$

where $M$is the molecular weight of N-mer; M_0 is the molecular weight of the monomer. Combining Eq. (1.4.1) and Eq. (1.4.10), the number of lattice sites occupied by the monomer c_0 is obtained as:

$$c_0 = M_0/\rho^* v^*. \tag{1.4.11}$$

The volume of an empty lattice site is also considered as v^*; then the volume of the system is therefore:

$$V = (N_0 + rN_1)v^* = N_r v^* = V^*/f. \tag{1.4.12}$$

To construct the Gibbs free energy, we still need to know the lattice energy E of this system. Sanchez and Lacombe consider that only the nearest-neighbor interactions contribute to the lattice energy, which can be mathematically expressed as [23]:

$$E = -(z/2)N_r \sum_{\substack{0 \le i \le m \\ 0<j<n}} P(i,j)\,\epsilon_{ij}, \tag{1.4.13}$$

where ϵ_{ij} is the pair interaction energy between components i and j; $P(i,j)$ is the probability of forming the pair. The zero pair interaction energy is associated with

hole-hole, hole-mer and bonded $\left(mer_i - mer_j\right)_{i=j}$ pairs. Only the energy of non-bonded $\left(mer_i - mer_j\right)_{i\neq j}$ interaction ϵ is not zero and the probability of a non-bonded interaction is [21]:

$$P\left(mer_i - mer_j\right)_{i\neq j} = (qN_1)^2/N_qN_r, \tag{1.4.14}$$

whose large z limit is

$$\lim_{z\to\infty} P\left(mer_i - mer_j\right)_{i\neq j} = (rN_1/N_r)^2 = f^2. \tag{1.4.15}$$

By combining Eq. (1.4.13) and Eq. (1.4.15), the lattice energy is obtained as:

$$E = -N_r(z\epsilon/2)f^2, \tag{1.4.16}$$

which can also be written as:

$$E/rN_1 = -\epsilon^* f, \tag{1.4.17}$$

where $\epsilon^* = z\epsilon/2$ is the total interaction energy per mer. Since E and Ω are functions of the single parameter N_0, the partition function evaluated by the mean field approximation can be expressed as a single sum over N_0:

$$Z(T,P) = \sum_{N_0=0}^{\infty} \Omega \exp[-\beta(E + PV)]. \tag{1.4.18}$$

Finally, the Gibbs free energy is obtained as:

$$G = -kT \ln Z(T,P) = E + PV - kT \ln \Omega, \tag{1.4.19}$$

which can be expressed in the dimensionless form:

$$G/Nr\epsilon^* \equiv \tilde{G} = -\tilde{\rho} + \tilde{P}\tilde{v} + \tilde{T}\left[(\tilde{v}-1)\ln(1-\tilde{\rho}) + \frac{1}{r}\ln(\tilde{\rho}/\omega)\right], \qquad (1.4.20)$$

where $\tilde{T}$, $\tilde{P}$, $\tilde{v}$ and $\tilde{\rho}$ are the reduced temperature, pressure, volume and density:

$$\tilde{T} \equiv T/T^*, \quad T^* \equiv \epsilon^*/k; \qquad (1.4.21)$$

$$\tilde{P} \equiv P/P^*, \quad P^* \equiv \epsilon^*/v^*; \qquad (1.4.22)$$

$$\tilde{v} \equiv 1/\tilde{\rho} \equiv V/V^*, \quad V^* \equiv N_1(rv^*). \qquad (1.4.23)$$

A pure fluid can be completely characterized by three molecular parameters: ϵ^*, v^* and r, or the equivalent scale factors T^*, P^* and ρ^*. The scale factors are related to the number of sites r occupied by the molecule and its molecular weight M by:

$$\frac{RT^*\rho^*}{P^*} = v^*\rho^* = M/r, \qquad (1.4.24)$$

$$\frac{P^*v^*}{RT^*} = 1. \qquad (1.4.25)$$

These parameters have been determined for different fluids by a nonlinear least-squares fitting of experimental vapor pressure data [30]. They are readily found in the literature [23, 30, 31] for a wide variety of fluids. The minimum values of Gibbs free energy can be found by:

$$\partial\tilde{G}/\partial\tilde{v}\big|\tilde{T},\tilde{P} = 0, \qquad (1.4.26)$$

which leads to the equation of state for this system:

$$\tilde{\rho}^2 + \tilde{P} + \tilde{T}\left[\ln(1-\tilde{\rho}) + \left(1 - \frac{1}{r}\right)\tilde{\rho}\right] = 0. \tag{1.4.27}$$

The solution can be obtained by rewriting Eq. (1.4.27) as:

$$\tilde{\rho} = 1 - \exp[-\tilde{\rho}^2/\tilde{T} - (1-1/r)\tilde{\rho} - \tilde{P}/\tilde{T}] \equiv h(\tilde{\rho}). \tag{1.4.28}$$

The bounds on the solution of this equation can be obtained by the tangency condition (related to the spinodal condition, with its physical meaning to be explained later):

$$\frac{\partial h(\tilde{\rho})}{\partial \tilde{\rho}} = \frac{\partial\left(1 - \exp[-\tilde{\rho}^2/\tilde{T} - (1-1/r)\tilde{\rho} - \tilde{P}/\tilde{T}]\right)}{\partial \tilde{\rho}} = \frac{\partial \tilde{\rho}}{\partial \tilde{\rho}} = 1, \tag{1.4.29}$$

which leads to:

$$\left(\frac{2\tilde{\rho}}{\tilde{T}} + 1 - \frac{1}{r}\right)\exp[-\tilde{\rho}^2/\tilde{T} - (1-1/r)\tilde{\rho} - \tilde{P}/\tilde{T}] = 1. \tag{1.4.30}$$

Combining Eq. (1.4.28) and Eq. (1.4.30), we can eliminate the $\tilde{P}$ to yield:

$$\frac{2\tilde{\rho}^2}{\tilde{T}} - \left(\frac{1}{r} - 1 + \frac{2}{\tilde{T}}\right)\tilde{\rho} + \frac{1}{r} = 0, \tag{1.4.31}$$

which has two solutions for $\tilde{\rho}$:

$$\widetilde{\rho_1} = \frac{1}{4}\tilde{T}\left[\left(\frac{1}{r} + \frac{2}{\tilde{T}} - 1\right) + \sqrt{\left(\frac{1}{r} - 1 + \frac{2}{\tilde{T}}\right)^2 - \frac{8}{\tilde{T}r}}\right], \tag{1.4.32}$$

$$\widetilde{\rho_2} = \frac{1}{4}\tilde{T}\left[\left(\frac{1}{r} + \frac{2}{\tilde{T}} - 1\right) - \sqrt{\left(\frac{1}{r} - 1 + \frac{2}{\tilde{T}}\right)^2 - \frac{8}{\tilde{T}r}}\right]. \tag{1.4.33}$$

The obtained $\widetilde{\rho_1}$ and $\widetilde{\rho_2}$ can be substituted into Eq. (1.4.27) respectively to get the reduced pressure-temperature relation of the spinodal condition:

$$\widetilde{P_1}(\tilde{T}, r) = -\widetilde{\rho_1}^2 - \tilde{T}\left[\ln(1-\widetilde{\rho_1}) + \left(1-\frac{1}{r}\right)\widetilde{\rho_1}\right], \tag{1.4.34}$$

$$\widetilde{P_2}(\tilde{T}, r) = -\widetilde{\rho_2}^2 - \tilde{T}\left[\ln(1-\widetilde{\rho_2}) + \left(1-\frac{1}{r}\right)\widetilde{\rho_2}\right], \tag{1.4.35}$$

where $\widetilde{P_1}(\tilde{T}, r)$ is associated with the "stability limit for liquid" and $\widetilde{P_2}(\tilde{T}, r)$ is

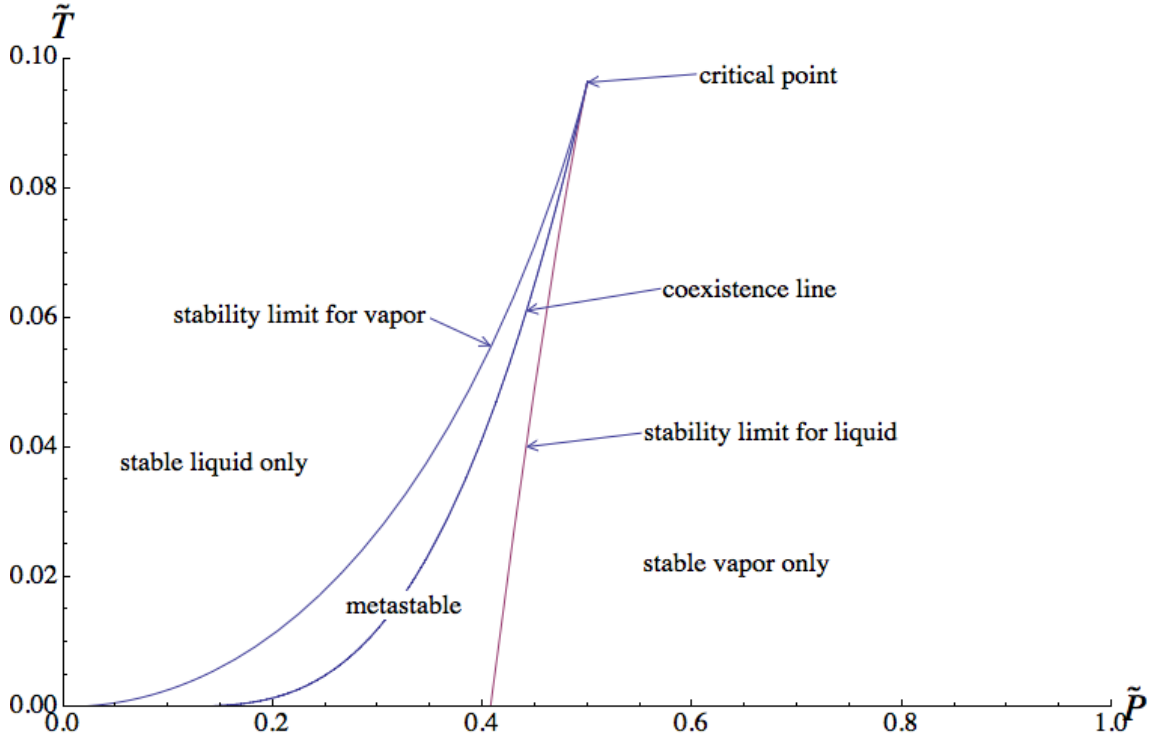

Figure 1.4.2: Reduced pressure-temperature diagrams for $r = 1$. Any $(\tilde{P}, \tilde{T})$ point inside the metastable region yields a free energy diagram with two minima similar to Fig. 1.4.4. Any $(\tilde{P}, \tilde{T})$ point on the coexistence line yields a free energy diagram with two equal minima similar to Fig. 1.4.7. Any $(\tilde{P}, \tilde{T})$ point outside the metastable region yields a free energy diagram with a single minima.

associated with the "stability limit for vapor" in Fig.1.4.2. Those two spinodal conditions are the two boundaries of the "metastable" region in Fig.1.4.2, which is quite useful in the numerical analysis of the equation of state for this system because it sets bounds on the solution of that equation. Any $(\tilde{P}, \tilde{T})$ point inside the "metastable" region yields three solutions for this equation as illustrated in Fig.1.4.3. The highest density minima is associated with a liquid-like phase while

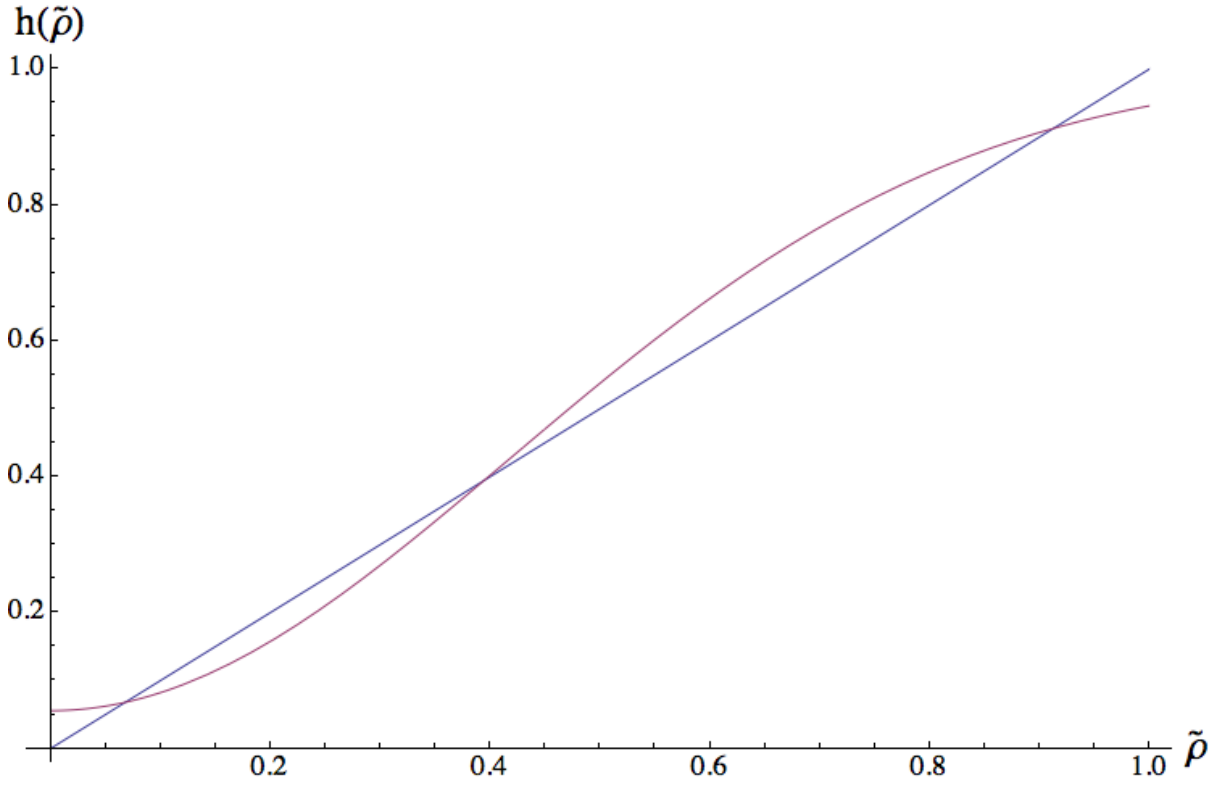

Figure 1.4.3: Schematic representation of the solutions of the equation of state (Eq.1.4.27). Values of parameters used in this calculation are: $r = 1, \tilde{P} = 0.02, \tilde{T} = 0.35$. Curves are plotted based on Eq.1.4.28. Solutions at the lowest and highest values of $\tilde{\rho}$ correspond to minima in $\tilde{G}$; the intermediate solution corresponds to a maximum in $\tilde{G}$. See Fig.1.4.4.

the lowest density corresponds to a vapor-like phase. Solutions at the lowest and highest values of $\tilde{\rho}$ are the two local minima in $\tilde{G}$; the intermediate solution corresponds to a maximum in $\tilde{G}$, as shown in Fig.1.4.4. If the pressure is increased isothermally, the vapor-like minimum disappears; if the pressure is decreased isothermally, the liquid-like minimum disappears. Similar behaviours apply if the temperature is increased or decreased isobarically [23]. In other words, the lattice fluid undergoes a liquid-vapor phase transition.

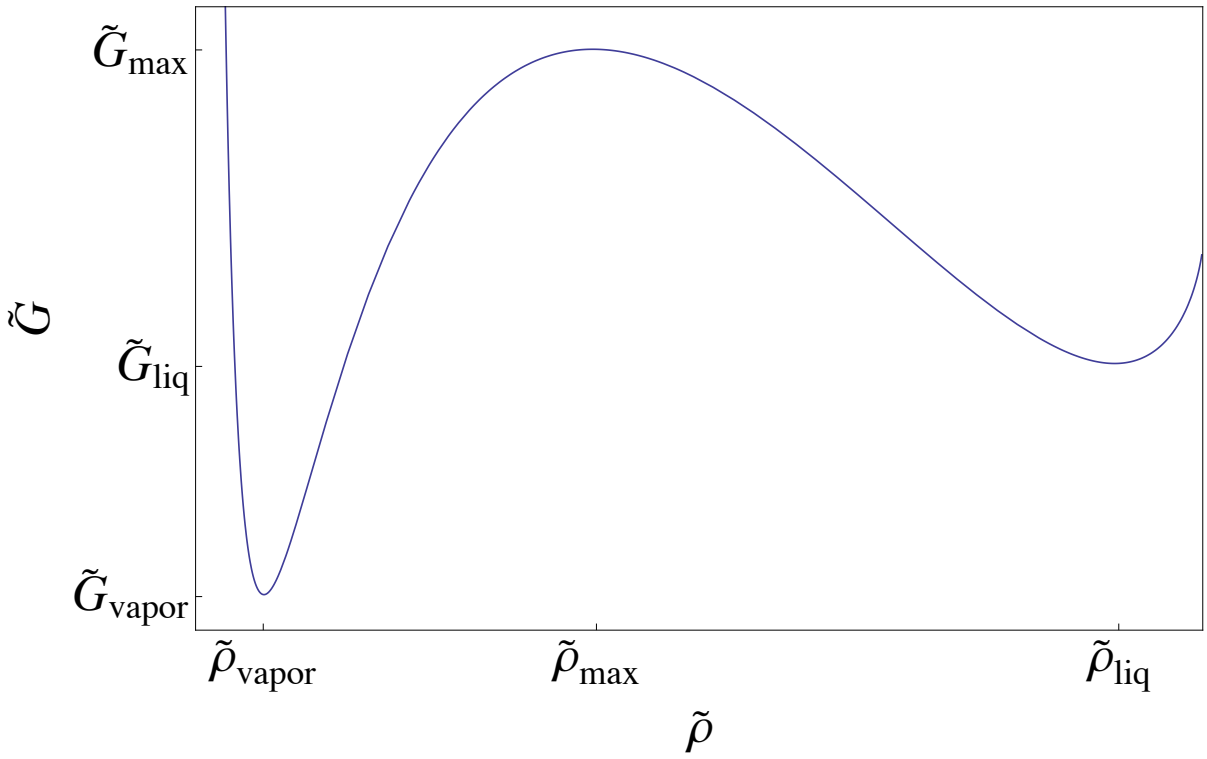

Figure 1.4.4: Reduced Gibbs free energy vs reduced density at a pressure and temperature where liquid-like phase is metastable with respect to the vapor-like phase. This curve is plotted based on Eq. (1.4.20) and parameters used in this calculation are the same as those used in Fig.1.4.3.

The higher local minimum of $\tilde{G}$ represents the metastable state, while the overall minimum of $\tilde{G}$ represents the equilibrium state. In this case, the equilibrium state corresponds to the vapor-like phase which has lower free energy. Any $(\tilde{P}, \tilde{T})$ point on the two boundaries of the "metastable" region yields two solutions for Eq. (1.4.26). The two boundaries obtained from the tangency condition are related to spinodal conditions, which define the metastability limit of a phase. As

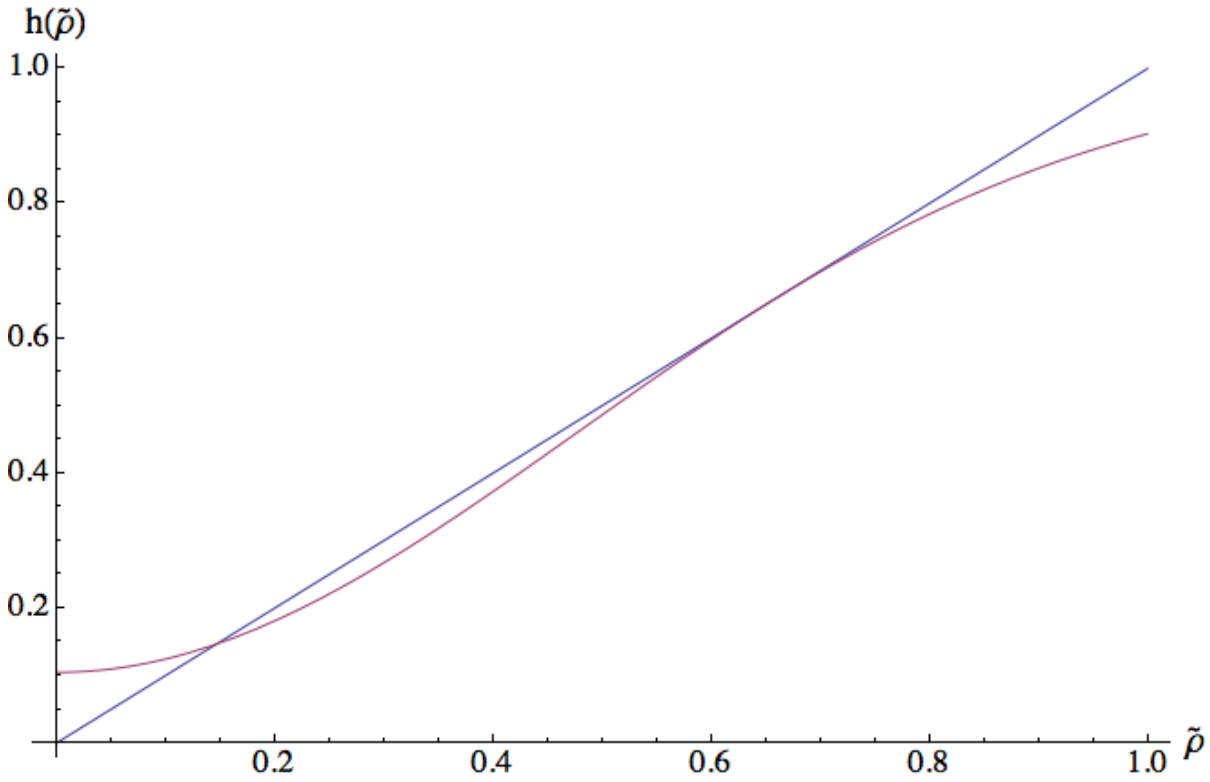

Figure 1.4.5: Schematic representation of the solutions of the equation of state (Eq.1.4.27). Values of parameters used in this calculation are: $r = 1$, $\tilde{T} = 0.45$. Curves are plotted based on Eq.1.4.28 and Eq.1.4.34. The solution at the lower $\tilde{\rho}$ correspond to minima in $\tilde{G}$; the solution at the higher $\tilde{\rho}$ corresponds to an inflexion point in $\tilde{G}$ curve. See Fig.1.4.6.

illustrated in Fig.1.4.5, one $(\tilde{P}, \tilde{T})$ point on the boundary of the "metastable" region indicated by "stability limit for liquid" in Fig.1.4.2 produces two solutions for Eq. (1.4.26). The solution at the lower $\tilde{\rho}$ is associated with the minimum of $\tilde{G}$, which represents the vapor-like phase. The solution at the higher $\tilde{\rho}$ denotes an inflexion point in $\tilde{G}$ curve, which represents the limit of the liquid–like phase, as shown in Fig.1.4.6. In other words, the liquid-like phase will disappear, if $(\tilde{P}, \tilde{T})$

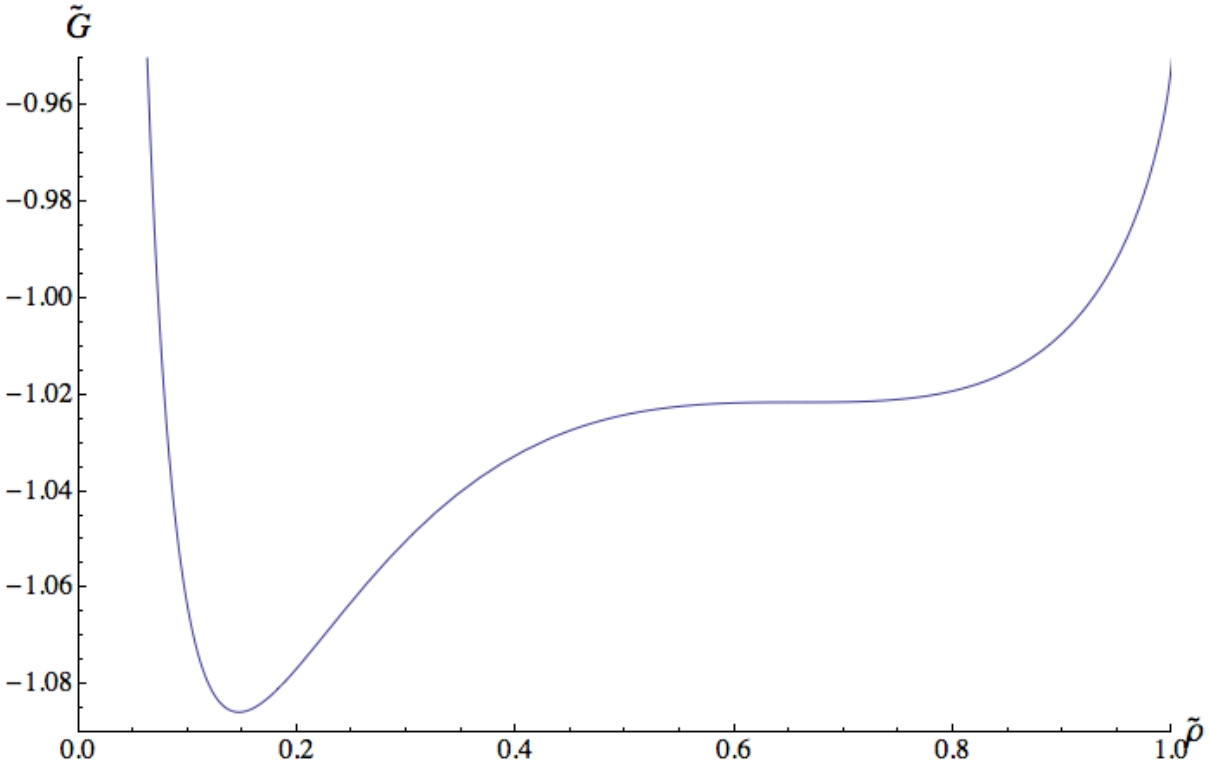

Figure 1.4.6: Reduced Gibbs free energy vs reduced density when $(\tilde{P}, \tilde{T})$ point is on the "stability limit for liquid" boundary of the "metastable" region . This curve is plotted based on Eq. (1.4.20) and parameters used in this calculation are the same as those used in Fig.1.4.5.

point moves to the “stable vapor only” region after crossing the boundary-“stability limit for liquid”. Vapor-like phase will have the same situation when the “stability limit for vapor” is considered. As a result, any $(\tilde{P}, \tilde{T})$ point outside the “metastable” region yields only one solution for Eq. (1.4.26). In a more specific case, at a given temperature there will be a situation when the free energy of vapor phase is equal to that of liquid phase as shown in Fig.1.4.7.

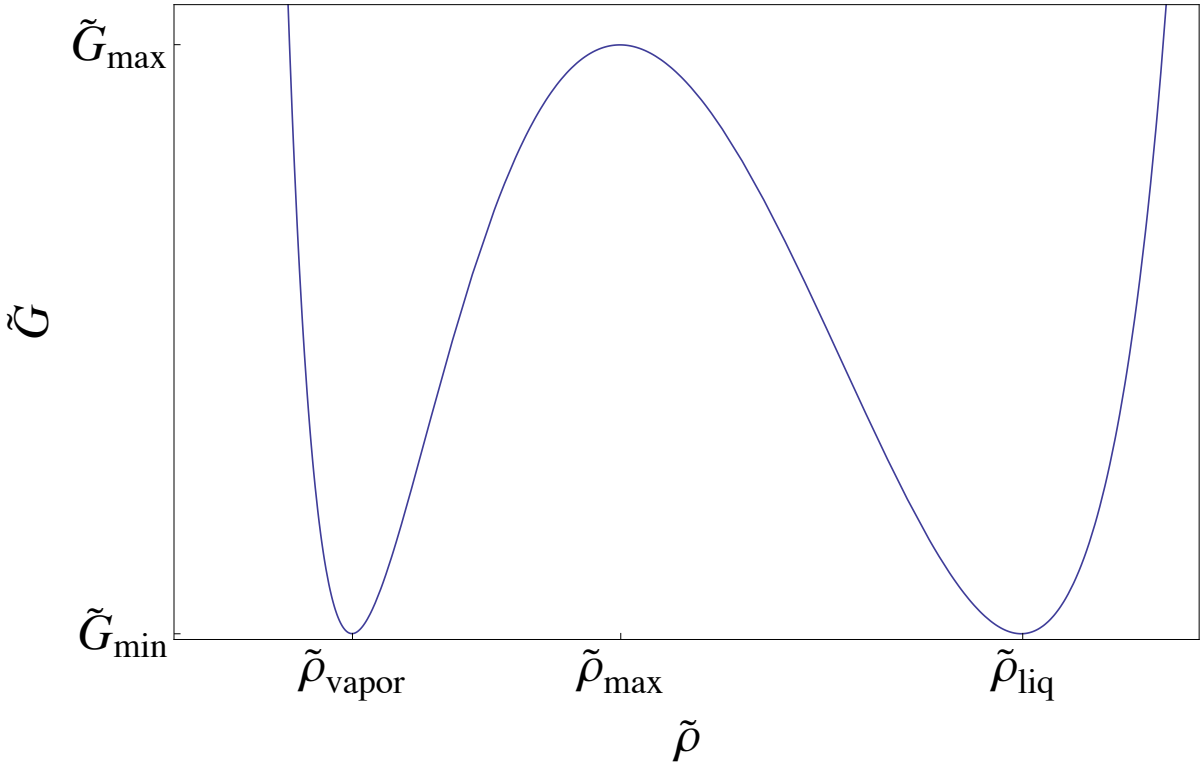

Figure 1.4.7: Binodal condition when Gibbs free energy values for the vapor-like phase and the liquid-like phase are equal.

This is referred to the binodal condition related to the “coexistence line" in the reduced pressure-temperature diagram. The binodal condition is the special case

of the equilibrium state when the vapor phase and liquid phase coexist. This temperature and pressure are defined as the saturation temperature and pressure (vapor pressure).

This Lattice-Fluid theory is a well developed statistical mechanical model and it predicts a liquid-vapor transition for pure polymer melts. Any molecular fluid can be described by only three scale parameters (T^*, P^*, ρ^*) and these parameters have been determined by the experimental data for many common fluids. Thus, this lattice model can be used to predict vapor pressures of a wide range of pure polymer melts. In this thesis, the vapor pressure of each N-mer polystyrene predicted by the Lattice-Fluid theory is employed to demonstrate the ability of the vacuum distillation. Another important parameter--the glass transition temperature--is used to estimate the molecular weight of N-mer polystyrene purified by the vacuum distillation. Section 1.5 will introduce basic properties of the glass transition of polymer and the free volume theory which deals with the effects of molecular weight on the glass transition.

1.5 Introduction to the glass transition of polymer

The nature of the glass transition is still an open question despite considerable efforts made by theoretical and experimental researchers. Last century, Flory and Fox [3] defined the glass transition process of polymer as “a second order

transition which is not an equilibrium transition in the thermodynamic sense but that originating from kinetic limitations on the rates of internal adjustments occasioned by changes in temperature". As the polymer is heated up, it transforms from the hard and brittle "glassy" state (at which polymer chains are locked in a tangled, coiled position) to the soft and ductile "rubbery" state (at which polymer chains are able to more easily rotate and slip past each other) [32]. Consequently, many physical properties of polymers change significantly when the glass transition occurs, e.g. density, shear modulus, refractive index, heat capacity. The behavior of the glass transition is quite different from those of other phase transitions, such as the crystallization, because, unlike crystallization, the changes in any of those physical quantities are not discontinuous in the glass transition [33]. Generally, a first-order phase transition involves discontinuous changes in the first derivatives of the Gibbs free energy, such as volume $V = \left(\frac{\partial G}{\partial P}\right)_T$ and entropy $S = -\left(\frac{\partial G}{\partial T}\right)_P$. The liquid-to-crystal transition is the first-order phase transition as it involves discontinuous changes in volume and entropy. However, the volume and entropy change continuously in the glass transition region. As depicted in Fig. 1.5.1, the volume and enthalpy with respect to temperature change abruptly but continuously at the transition temperature T_{ga}

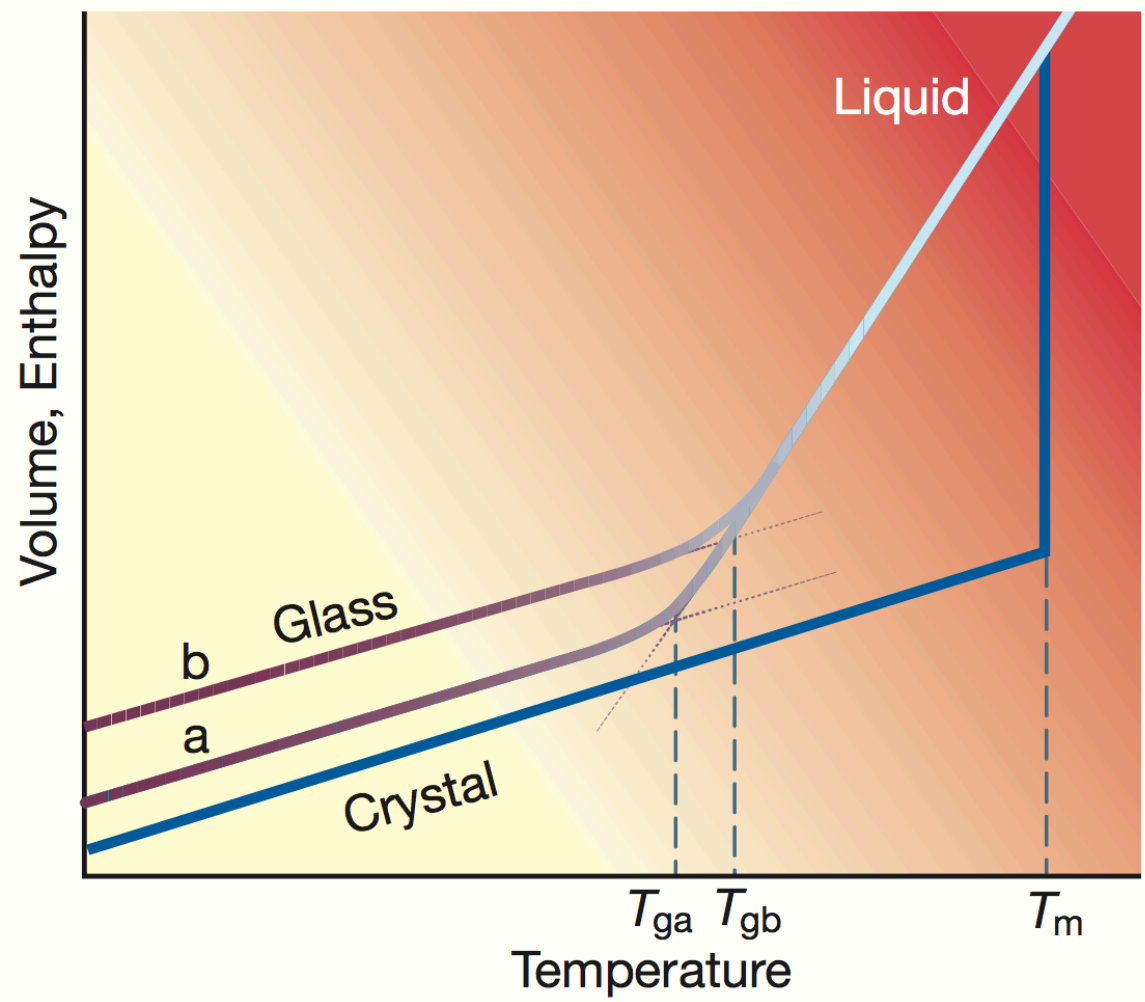

Figure 1.5.1: Temperature dependence of a liquid's volume or enthalpy at constant pressure. The liquid-equilibrium state is denoted as the white straight line. The transition curve of crystallization is denoted as the blue polyline. T_m is the melting temperature. A slow cooling rate produces a glass transition at T_{ga}; a faster cooling rate leads to a glass transition at T_{gb}. Figure from Ref. [33].

and T_{gb}, while the discontinuous transition occurs at the melting temperature T_m.

A second order phase transition as defined by Ehrenfest [34] is one for which the second derivatives of the Gibbs free energy, such as heat capacity $C_p =$

$-T\left(\frac{\partial^2 G}{\partial T^2}\right)_P$ and thermal expansion coefficient $\alpha = \frac{1}{V}\left(\frac{\partial}{\partial T}\left(\frac{\partial G}{\partial P}\right)_T\right)_P$, are discontinuous through the transition. An archetypal example of second order phase transition is the paramagnetic-to-ferromagnetic phase transition. An illustrative example of this is that there is discontinuity in magnetization of iron or nickel as the magnetic field goes through zero below a Curie temperature [35]. At this point, the glass transition is more like the second order transition, since the second derivatives of the Gibbs free energy, such as thermal expansion coefficient and heat capacity, exhibit discontinuous changes in the glass transition region [3]. The intersection of the liquid and vitreous portions of the volume versus temperature curve provides one definition of glass transition temperature (T_g), which usually occurs around $\frac{2}{3}T_m$[33]. Crystallization can be avoided if the cooling rate is fast enough, since the molecules do not have adequate time to rearrange the configurations. Slower cooling rate leads to a lower T_g, because of a longer time available for sampling configurations at each temperature, which makes the liquid cooler before it falls out of the liquid-equilibrium state. Experimentally, T_g changes by 3~5 ℃ when cooling rate changes by an order of magnitude. In this thesis, the same cooling rate as described in Section 2.4 is employed to eliminate deviations of T_g caused by

different cooling rates. Different fast cooling rates lead to different glassy states in terms of different arrangements of molecules, which trend to evolve toward the final equilibrium states. During the glass transition, there is small change in molecular potential energy, but there are dramatic changes in molecular motions, which suggests that the glass transition is related more to a type of kinetic arrest phenomena [36,37] than to a thermodynamic phase transition.

Several theories have been established to explain the unique phenomenon near the glass transition temperature and one of them is the free volume theory, which is reasonably straightforward to understand. In the free volume theory, Flory and Fox [3] first proposed that the specific volume v in liquids contains the occupied volume v_0 and free volume v_f, where the free volume v_f is the volume of holes between the chain segments and is a constant independent of both molecular weight and temperature below T_g. The occupied volume v_0 is given by:

$$v_0 = A_0 + (dv/dT)_1 T, \tag{1.5.1}$$

where A_0 is the hypothetical volume of the glass at $T = 0$ ℃ and $(dv/dT)_1$ is the glass expansion coefficient below T_g. Thus, the free volume v_f can be written as:

$$v_f = v - v_0 = v - A_0 - (dv/dT)_1 T. \tag{1.5.2}$$

The end groups of the polymer usually act like a foreign substance in disrupting the local configurational order of monomer units, and this is manifested by an increase in the specific volume v which is proportional to the concentration of end groups, or to $1/\overline{M_n}$ [3]. The specific volume v above T_g can be written as:

$$v = A_1 + (dv/dT)_2 T + B/\overline{M_n}\,, \tag{1.5.3}$$

where A_1 and B are constants, and $(dv/dT)_2$ is the glass expansion coefficient above T_g. Subtracting Eq. (1.5.2) from Eq. (1.5.3), we obtain:

$$v_f = A_f + [(dv/dT)_2 - (dv/dT)_1]T + B/\overline{M_n}\,, \tag{1.5.4}$$

where $A_f = A_1 - A_0$. Using the requirement that the equilibrium free volume of the polymer of molecular weight $\overline{M_n}$ at its transition temperature T_g be equal to that of one for which $\overline{M_n} = \infty$ at its transition temperature $T_{g,\infty}$, then we get:

$$T_g = T_{g,\infty} - B/\{[(dv/dT)_2 - (dv/dT)_1]\overline{M_n}\}\,, \tag{1.5.5}$$

which can be simplified as:

$$T_g = T_{g,\infty} - K/\overline{M_n}\,, \tag{1.5.6}$$

where K is a constant. This expression relating the T_g to the molecular weight is generally accepted and is well known as Fox-Flory relation.

1.6 Conclusion

In conclusion, this chapter has introduced the polydispersity index that signifies the degree of impurity for polymers. Then, I reviewed the physical technologies for purification of polymers with vacuum distillation fractionation argued to have the potential ability of separating polymers larger than 3-mer. Chapter 2 will introduce a home-made apparatus to further explore vacuum distillation fractionation of polymers. This chapter has also introduced a lattice fluid theory of pure polymer melts, which will facilitate to calculate vapor pressures of pure N-mers in Chapter 3. Finally, free volume theory for the glass transition of polymer is introduced. Fox-Flory relation obtained from free volume theory predicts that T_g of polymers decreases linearly with $1/\overline{M_n}$. In this thesis, T_g obtained from the same cooling rate is used to estimate the molecular weight of the purified polystyrene and Chapter 2 will describe the measurement of T_g.

2. Experimental Techniques

2.1 Introduction

In this chapter, sample preparation for the experiment is first introduced. Then home-made thermal vacuum apparatus for evaporative purification is designed and constructed so as to explore the potential ability of vacuum fractional distillation discussed in Section 1.3. Finally, I will introduce basic components and working principles of Differential Scanning Calorimeter, and how it can be used to measure the glass transition temperature of polystyrene.

2.2 Sample Preparation

Polydisperse polystyrene as a familiar polymer with a wide range of commercial issues is chosen as starting material in evaporative experiment. Experiments in this thesis are based on two types of polydisperse polystyrenes: PS with $\overline{M_w} = 600\ g/mol$ & $890\ g/mol$ synthesized by anionic polymerization, and PS with $\overline{M_w} = 1200\ g/mol$ synthesized by free radical polymerization. This section will introduce sample pre-treatment of these materials.

80 mg polydisperse polystyrene sample is placed on a flat substrate-a squared polished Si wafer of 0.3 mm thickness and 1.4 cm side length. The substrate is

then heated on a Linkam stage in a vacuum chamber at temperature 80 ℃ for several minutes until a uniform liquid layer is formed.

The vertical temperature gradient caused by non-uniform thickness of initial sample is minimized by this pre-treatment. The prepared sample will then be purified by the thermal vacuum apparatus as described in Section 2.3.

2.3 Vacuum system of thermal evaporation

The thermal vacuum apparatus is designed for the short path vacuum distillation technique which involves a short distance (usually a few mm comparable to mean free path of vapor molecules in high vacuum) from evaporator to condenser. The short path vacuum distillation is a preferred technique for materials (such as polymers) unstable at high temperature because this technique is operated at lower temperature which causes least thermal decomposition of materials [38]. The construction of the apparatus is described as below.

If the area of the sample substrate exceeds that of circular heating stage with 2 cm diameter, a significant temperature gradient along radial direction will occur near edges of the substrate due to indirect contact with the heater. As a consequence, different molecular weight N-mers are evaporated at different temperature, which reduces the purity of the deposition product. To minimize this

temperature gradient, the side length of a square sample substrate is designed as 1.4 cm to ensure entire sample substrate can directly contact with the heater. The removable substrate (usually a squared polished Si wafer of 5 cm side length) as

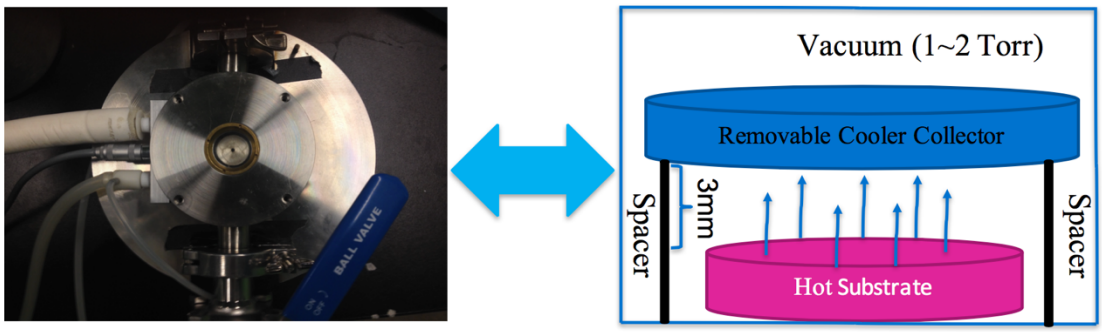

Figure 2.3.1: Top view of thermal vacuum apparatus (left); side view of the thermal vacuum apparatus (right). The apparatus consists of vacuum pump, spacers, removable collector, and Linkam heating stage integrated with proportional-integral-derivative temperature controller.

a condenser of collecting deposited polystyrene is separated from the deposition source by spacers (four screws) of 3 mm. The vacuum chamber is evacuated with an Agilent technologies SH-110 dry scroll pump with an ultimate pressure of 0.05 Torr. When heating in such high vacuum, temperature fluctuation of 5 ℃ is observed even when the liquid nitrogen enhanced proportional-integral-derivative Linkam temperature controller is employed, which is caused by vacuum thermal isolation limiting heat transfer on sample surface. At this point, nitrogen gas is admitted to the chamber until the ambient pressure is about 1~2 Torr. This small pressure gas enhances heat exchange between the surface of the

heating stage and the sample. As a result, the temperature control becomes much more stable. Since spacers are not in contact with the hot substrate and the thermal isolation caused by the vacuum, the top substrate can be cool enough to collect the majority of evaporated materials.

The deposition product of this short-path apparatus is then transferred to a sample pan for the measurement of T_g as introduced in the following section.

2.4 Differential scanning calorimeter (DSC)

As mentioned in Section 1.5, the molecular weight of polystyrene can be estimated by T_g based on the Fox-Flory relation. T_g values also reflect the purity of deposited polystyrene, which will be discussed in Section 4.2. This section will introduce how to measure T_g values of polystyrenes.

The T_g values of polystyrene samples obtained in this thesis are measured by a TA Instruments Q100 Differential Scanning Calorimeter (DSC). The polystyrene sample is first pressed in a premium hermetic pan (with serial number: 901683.901); then this sample pan and an empty reference pan are placed on small platforms within the DSC chamber which is full of nitrogen gas. As shown in Fig.2.4.1, the platforms are heated by the thermoelectric disc and the temperature is measured by the thermocouple sensors. A refrigerator is integrated

with the system as the cooling system. The DSC is operated at a cooling rate of 10 K/min to measure the T_g values of our samples. The signals of the temperature and heat flow are monitored by the computer programs.

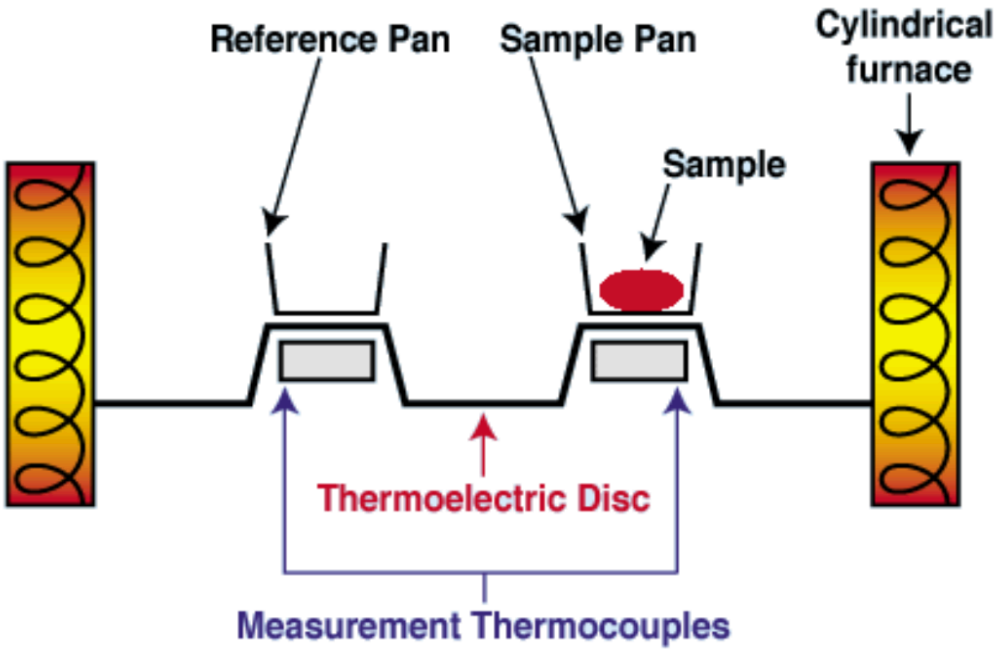

Figure 2.4.1: Schematic of the interior of a DSC. Thermoelectric disc as temperature controller is powered by cylindrical furnace. Thermocouple sensor below reference/sample pan monitors temperature of that pan. The DSC ultimately outputs the differential heat flow between material and the empty reference pan. Figure from *Operation Manual of TA Instruments Q100 DSC*.

The specific heat C_p and heat flow q have the following relation:

$$C_p = \frac{q}{\Delta T} \qquad (2.4.1)$$

where C_p is the material's heat capacity, q is the heat flow ($J/(s \cdot g)$) through the material over a given time, and ΔT ($℃/s$) is the change in temperature over that same time. Since the specific heat C_p of a polymer changes abruptly at the

glass transition temperature and the heat flow q from the DSC is proportional to C_p [39], DSC is an ideal instrument to characterize the T_g.

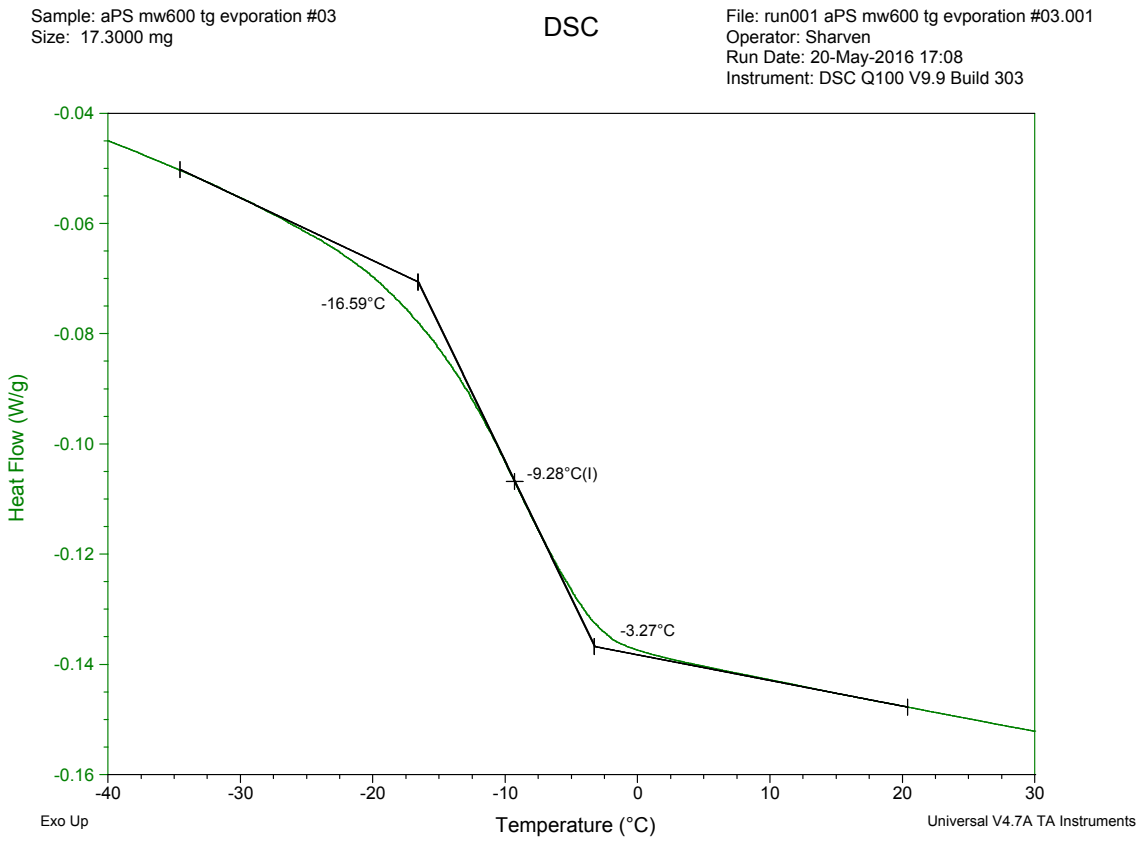

Figure 2.4.2: Determination of T_g from DSC curve. T_g measurement of $\overline{M_w} = 600\ g/mol$ polystyrene with $\overline{M_w}/\overline{M_n}$=1.2 by Q100 DSC operated at 10 ℃$/min$ cooling rate. The inflexion point of the function curve is associated with T_g value and it is calculated by Analysis Software of Universal V4.7A TA Instruments via the first derivative of the glass transition curve. For this data, T_g is -9.28 ℃, which locates at the midpoint of the incline.

Fig.2.4.2 shows the determination of T_g based on the heat flow-temperature curve. It is notable that the change of heat flow near the glass transition region occurs within a temperature range. At this point, we usually take the midpoint of

the incline as the T_g, since a plot of the first derivative of the glass transition curve shows a peak at the midpoint, which makes this point easy to identify.

2.5 Conclusion

In conclusion, this chapter gives a brief introduction to DSC as well as its working principle of measuring T_g of polymers. This chapter also describes a home-made apparatus for short path vacuum distillation and its ability of purifying polydisperse polystyrenes will be tested through experiments in Chapter 4. Numerical work of guiding experiments in Chapter 4 will be introduced first in Chapter 3.

3. Numerical simulations of polystyrene purification by evaporation

3.1 Introduction

In this chapter, numerical calculations of the vapor pressure of pure polystyrene based on the lattice fluid theory is described. To predict the purity of polystyrene purified by evaporation, a mass transport relation for mixture is then carried out to simulate the polydispersity index of purified polystyrene.

There have been a number of studies which have purified polymers into more monodisperse samples by using different fractionation techniques. Those studies usually involve vacuum distillation of dimers and trimers [12], and other chromatographic techniques [13,18-19], or solvent fractionation [13,18] for larger *N*. As mentioned in Section 1.3, quantities of *N*-mers (larger than 3-mer) produced by those techniques are limited at the milligram level and it is also clear that the fractionated components of these studies are mixed with the solvents and are still mixtures. Evaporative purification is essentially an application of short path distillation. We are extending what others have done for the dimer and trimer to cover a much larger range of *N* (up to 13-mer for polystyrene)-limited only by the temperature at which thermal decomposition would occur.

3.2 Vapor pressure of polystyrene as a function of molecular weight and temperature

To demonstrate how evaporative purification works, we need to know the vapor pressure of each *N*-mer. Since these vapor pressures have not yet been measured so far, we calculate their values through numerical simulations based on the lattice fluid theory introduced in Section 1.4. In this lattice fluid theory of a pure polymer melt, the equation of state for the system is expressed as:

$$\tilde{\rho}^2 + \tilde{P} + \tilde{T}\left[\ln(1-\tilde{\rho}) + \left(1-\frac{1}{r}\right)\tilde{\rho}\right] = 0 \qquad (3.2.1)$$

where $\tilde{\rho}$, $\tilde{T}$ and $\tilde{P}$ are the reduced density , temperature and pressure:

$$\tilde{\rho} = \frac{\rho}{\rho^*} \qquad \tilde{T} = \frac{T}{T^*} \qquad \tilde{P} = \frac{P}{P^*} \qquad (3.2.2)$$

These reduced parameters can be converted to real physical values ρ, T and P, once the characteristic parameters ρ^*, T^* and P^* are given. In the simulation, the characteristic values of polystyrene are: $\rho^* = 1105\, kg/m^3$, $T^* = 735$ K, $v^* = 17.1\, cm^3/mol$ and $P^* = 357000000\, P_a$ as found in Table II from Ref. [30]. Based on Eq. (1.4.10) in Section 1.4, r related to N for polystyrene is obtained as:

$$r = \frac{M_0}{\rho^* v^*} N = \frac{104\, g/mol}{1.105\, g/cm^3 \times 17.1\, cm^3/mol} = 5.5N \qquad (3.2.3)$$

As introduced in Section 1.4, the vapor pressure is defined by the binodal condition in which case the vapor phase and liquid phase coexist due to their equal Gibbs free energy. However, unlike the spinodal conditions which have solvable solutions as shown in Eq. (1.4.31) and Eq. (1.4.32), there is no analytic

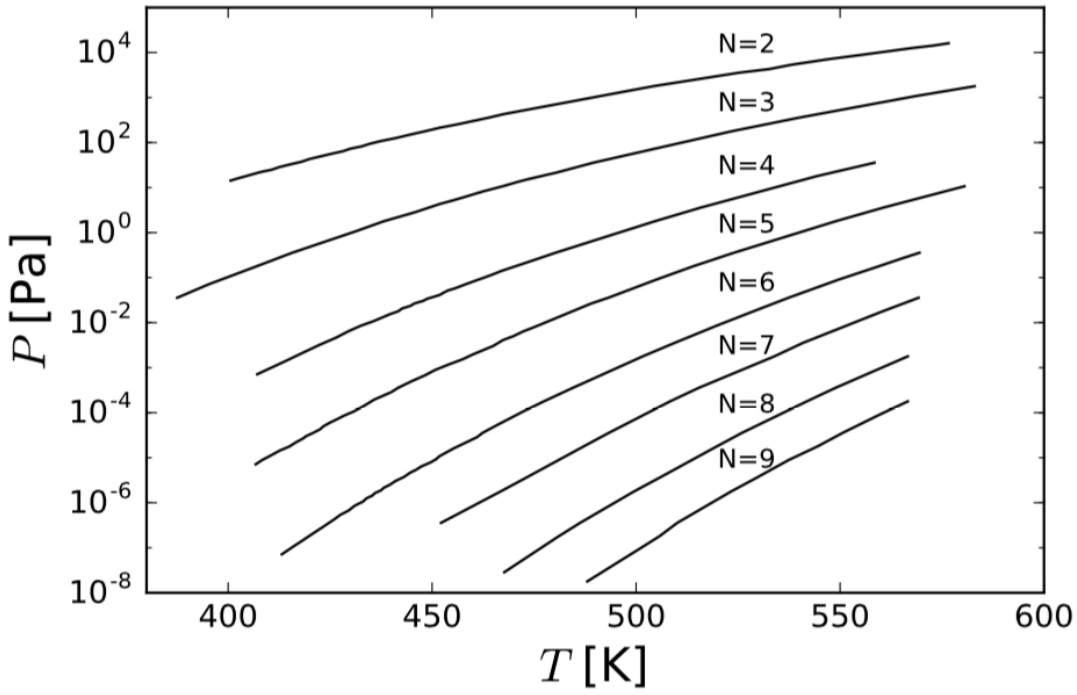

Figure 3.2.1: Calculated vapor pressures for polystyrene *N*-mers as a function of temperature and polymerization index *N*. The reduced pressure $\widetilde{P}$ and temperature $\widetilde{T}$ have been converted to real physical values.

solution for the binodal condition. At this point, numerical simulation is employed to find saturation points $(\tilde{P}, \tilde{T})$ consisting the "coexistence line" of the binodal condition. For each *N*-mer, at a given pressure there will be a unique temperature at which the two minimal values of Gibbs free energy are equal. In order to find

these saturation points $(\tilde{P}, \tilde{T})$ efficiently, a value of the pressure is set within the two boundaries defined by spinodal conditions and then a series of temperature is traversed to search a saturation temperature. A saturation point $(\tilde{P}, \tilde{T})$ is then selected, when the two minimal values of Gibbs free energy are closest to each other. The vapor pressure as a function of temperature can be plotted based on the locus of all such saturation points for N-mer polystyrenes with N ranging from 2 to 9, as shown in Fig.3.2.1. The difference between the vapor pressure of N-mer and that of $(N+1)$-mer is generally 2 orders of magnitude, which shows the vapor pressure of each N-mer is strongly dependent on the polymerization index. This strong dependence on N is valid for polystyrenes, because r will change by 5.5 when N only changes by 1. The magnified change of r results from significant large molecular weight of styrene monomer $M_0 = 104\ g/mol$ based on Eq. (3.2.3). For polymers with lower molecular weight of monomer, such as polyethylene glycol with $M_0 = 44\ g/mol$, the dependence on N for vapor pressures becomes weaker. The calculated result also shows that the vapor pressure of each N-mer polystyrene has approximate one order of magnitude change when the temperature changes by 20 K, for example, the vapor pressure of 6-mer at 413 K is calculated as $7.14\times10^{-8}\ Pa$ and it will increase to $1.07\times10^{-6}\ Pa$ at 433 K.

Based on the calculated result, the vapor pressure decreases dramatically with increasing N at a given temperature. It becomes more difficult to vaporize a higher molecular weight polymer due to the required higher temperature. The highest molecular weight *N*-mer that can be vaporized is limited by the eventual thermal decomposition temperature, which will be demonstrated via experiments in Chapter 4. These calculations are probably not that quantitatively accurate for the actual values because the end groups of polymer chains are not considered when we calculate N, but the strong dependence on N is expected to be reliable (since N-mers in a single polydisperse sample used in this thesis have the same end group that causes the same deviation of r value for each N-mer) and it still should be a good prediction to guide experiments.

3.3 Polydispersity index (PDI) of purified polystyrenes based on molar fractions and evaporation rates

To demonstrate how the evaporative purification technique works for the mixture, the vapor pressure of the single N-mer calculated above is not enough and we still need to know the partial vapor pressure of each N-mer in the mixture. In the simulation, the relation between the vapor pressure of the single N-mer and the partial vapor pressure of that N-mer is established by the Raoult's law. Meanwhile, based on the Langmuir evaporation equation that connects the partial vapor

pressure and the evaporation rate, a new mass transport relation is proposed in this thesis to predict the PDI of purified polystyrenes. The Langmuir evaporation equation and Raoult's law are described as below:

Langmuir evaporation equation

The Langmuir evaporation equation describes the relation between vapor pressure and evaporation rate for a mono-molecular liquid, such as pure metal melts or water. Irving Langmuir derived this equation to demonstrate the vapor pressure of metallic tungsten in vacuum [40] and the derivation proceeds as follow:

The metal is considered as one boundary surface of a unit cube of vapor. We can calculate the rate at which the vapor comes into contact with the metal. At the equilibrium state, half of the molecules in this unit volume are moving towards the metal while the other half are moving away from it. Let ρ be the density of the vapor, then the mass of gas moving towards the metal is $\frac{1}{2}\rho$. If the average velocity of the molecules is assumed to be $\bar{v}$, then the average component of the velocity in any given direction is $\frac{1}{2}\bar{v}$. Thus, the mass of gas which moves away from the unit surface of metal per second is obtained as:

$$\frac{dm}{dt} = \frac{1}{2}\rho\frac{1}{2}\bar{v} = \frac{1}{4}\rho\bar{v} \,. \qquad (3.3.1)$$

By introducing the ordinary gas law $PV = RT$, the density ρ can also be written as:

$$\rho = \frac{M}{V} = \frac{MP}{RT} \qquad (3.3.2)$$

where P, M, T and R are pressure, molecular weight, absolute temperature and gas constant respectively.

By combining Maxwell's theory of the distribution of particle velocities in an ideal dilute gas $P = \frac{\pi}{8}\rho\bar{v}^2$ and Eq. (3.3.2), the average velocity can be further expressed as:

$$\bar{v} = \sqrt{\frac{8RT}{\pi M}}\,. \qquad (3.3.3)$$

Substitute Eq. (3.3.3) and Eq. (3.3.2) in Eq. (3.3.1), we obtain the evaporation rate:

$$\frac{dm}{dt} = P\sqrt{\frac{M}{2\pi RT}}\,. \qquad (3.3.4)$$

Eq. (3.3.4) shows the desired relation between the vapor pressure and the evaporation rate in vacuum. In reality, molecules evaporated from the source into free space will likely collide with other vapor molecules and a portion of vapor molecules are reflected back to the source, thus the condensation coefficient γ is usually introduced to modify evaporation rate [41]. Langmuir evaporation equation can be eventually expressed as:

$$\frac{dm}{dt} = \gamma P\sqrt{\frac{M}{2\pi RT}}\ (0 < \gamma \leq 1)\,. \qquad (3.3.5)$$

Raoult's law

Raoult's law [42] is a thermodynamics law which states that the partial vapor pressure of each component of an ideal mixture of liquids is equal to the vapor

pressure of the pure component multiplied by its mole fraction in the mixture.

Mathematically, it is described as:

$$P_i = P_i^* x_i \tag{3.3.6}$$

where P_i is the partial vapor pressure of the *i*-th component in the gaseous mixture; P_i^* is the vapor pressure of the *i*-th pure component and x_i is the mole fraction of the *i*-th component in the mixture.

Mass transport of a single component in a mixture

In this thesis, the mass transport relation for a single N-mer in the mixture is constructed by combining the Langmuir equation and Raoult's law resulting in the following expression:

$$\frac{dm_N}{dt} = -\gamma \frac{n_N}{\sum n_N} P_N \sqrt{\frac{M_N}{2\pi RT}}, \tag{3.3.7}$$

$$\frac{d(M_N n_N)}{dt} = -\gamma \frac{n_N}{\sum n_N} P_N \sqrt{\frac{M_N}{2\pi RT}}, \tag{3.3.8}$$

$$\frac{dn_N}{dt} = -\gamma \frac{n_N}{\sum n_N} P_N \sqrt{\frac{1}{2\pi RTM_N}} = -\gamma \frac{n_N}{\sum n_N} P_N \sqrt{\frac{1}{2\pi RTNM_0}}, \tag{3.3.9}$$

$$\frac{dn_N}{dt} = -\alpha \frac{n_N}{\sum n_N} P_N \sqrt{\frac{1}{TN}}, \tag{3.3.10}$$

where m_N is the mass of component with polymerization index N; n_N is the mole number of N-mer; $\frac{n_N}{\sum n_N}$ is the mole fraction of the that N-mer; P_N is the vapor pressure of N-mer as calculated in Fig. 3.2.1; $M_N = NM_0$ is the molecular weight

of N-mer and $\alpha = \gamma\sqrt{\frac{1}{2\pi R M_0}}$ is a constant dependent on monomer molecular weight M_0 and the condensation coefficient γ. The time scale of the evaporation is determined by the constant α in the simulation. These coupled mass transport

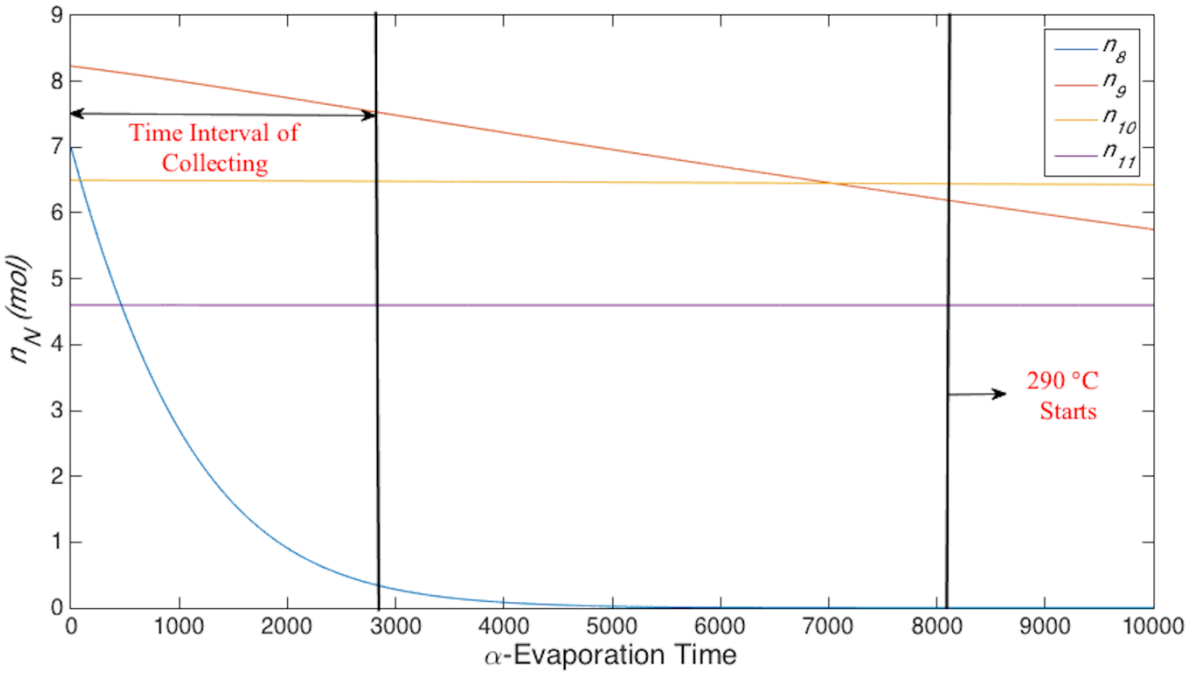

Figure 3.3.1: The mole number of *N*-mer polystyrene in mixture as a function of evaporation time at temperature 270℃ for *N*=8~11, which is calculated from Eq. (3.3.10). "α-Evaporation Time" denotes that the real time scale of evaporation is determined by the constant α, which will be further determined by experiment. The value of α is set as 10^4 for simplicity of the simulation.

equations are used to simulate the deposition process for the purification. Initially, the polystyrene mixture contains 11 components (N=1~11) with Gaussian distribution of molecular weight and $\overline{M_w}/\overline{M_n} = 1.18$, as shown in Fig.3.3.3. The evaporation starts at low temperature (130 ℃ in this simulation) and products of

evaporation are collected. When the evaporation rate falls below a certain value, the temperature is increased by 20 ℃. The purpose of the 20 ℃ increase in temperature is to improve the time efficiency of purification by producing approximate an order of magnitude change (estimated from calculated $P-T$ curves in Fig.3.2.1) in vapor pressure, since simulations suggest the time scale

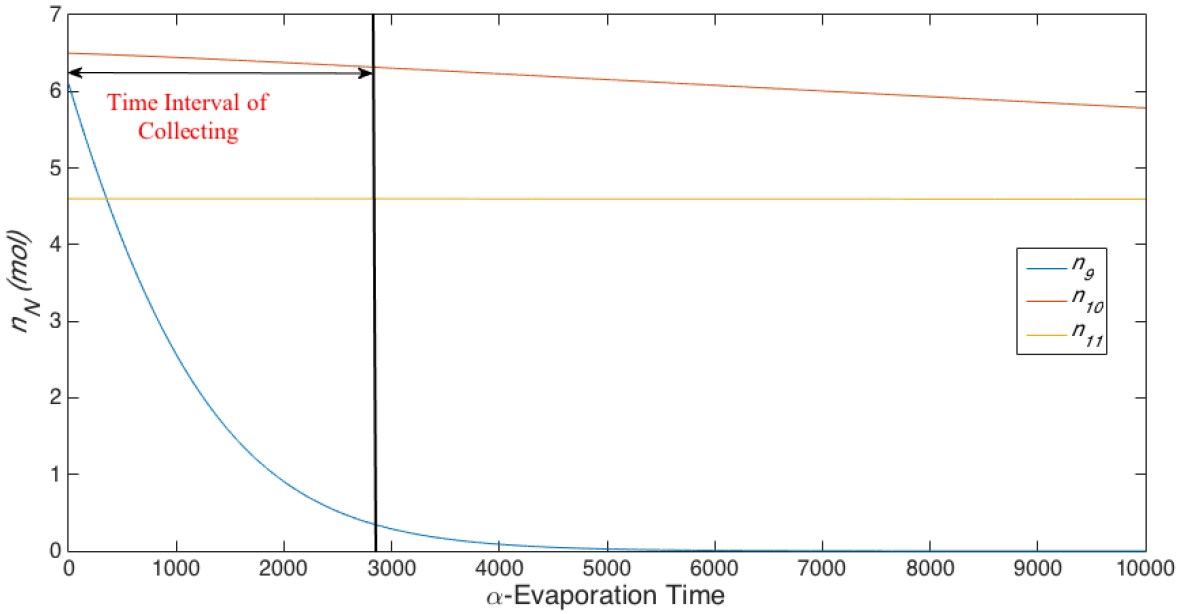

Figure 3.3.2: The mole number of *N*-mer polystyrene in mixture as a function of evaporation time at temperature 290℃ for *N*=9~11, which is calculated from Eq. (3.3.10). "α-Evaporation Time" denotes that the real time scale of evaporation is determined by the constant α, which will be further determined by experiment. The value of α is set as 10^4 for simplicity of the simulation.

required for continuous isothermal purification of the next higher molecular weight component is prohibitive. At the next higher temperature, the first separated component will not be collected until the previous lower molecular weight component can be totally evaporated off. Then the process is repeated. As shown

in Fig.3.3.1, when the temperature is increased to 270 ℃, there are 4 components left in the mixture. There is a large decrease for the amount of 8-mer and a small decrease for that of 9-mer, while amounts of 10-mer and 11-mer are almost constant. Evaporated materials are collected until the amount of 8-mer reduces to

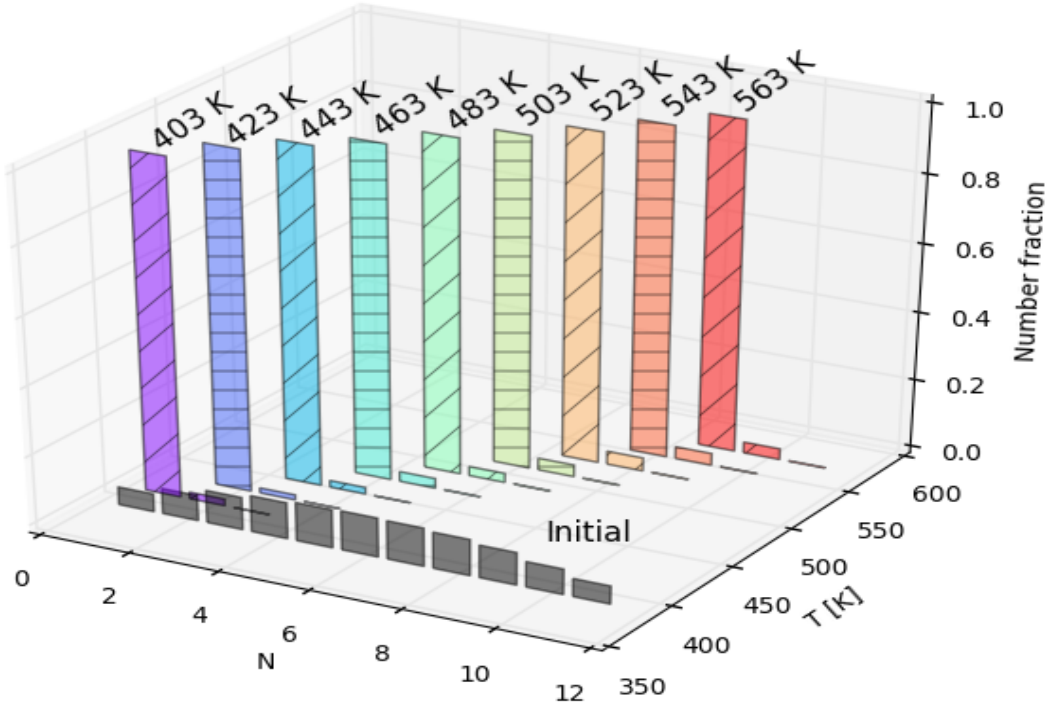

Figure 3.3.3: Initial molecular weight distribution of polystyrene mixture, and products after simulated evaporative purification method described in the text. Mole numbers of initial N-mer polystyrenes are set as $n_1 = n_{11} = 4.6\,mol$, $n_2 = n_{10} = 6.5\,mol$, $n_3 = n_9 = 8.3\,mol$, $n_4 = n_8 = 9.25\,mol$, $n_5 = n_7 = 9.8\,mol$, $n_6 = 10\,mol$, with mole number fractions following Gaussian distribution.

5% of its initial mole number in the mixture. Then the temperature is increased to 290 ℃ when 8-mer is almost exhausted. The same procedure is repeated at 290

℃ to separate 9-mer as shown in Fig.3.3.2. Eventually, the majority of single *N*-mer is separated at each temperature. As the histogram in Fig.3.3.3 shows, each purified product contains more than 95% *N*-mer and less than 5% impurity of (*N*+1)-mer and (*N*+2)-mer. The relevant polydispersity index of each separated

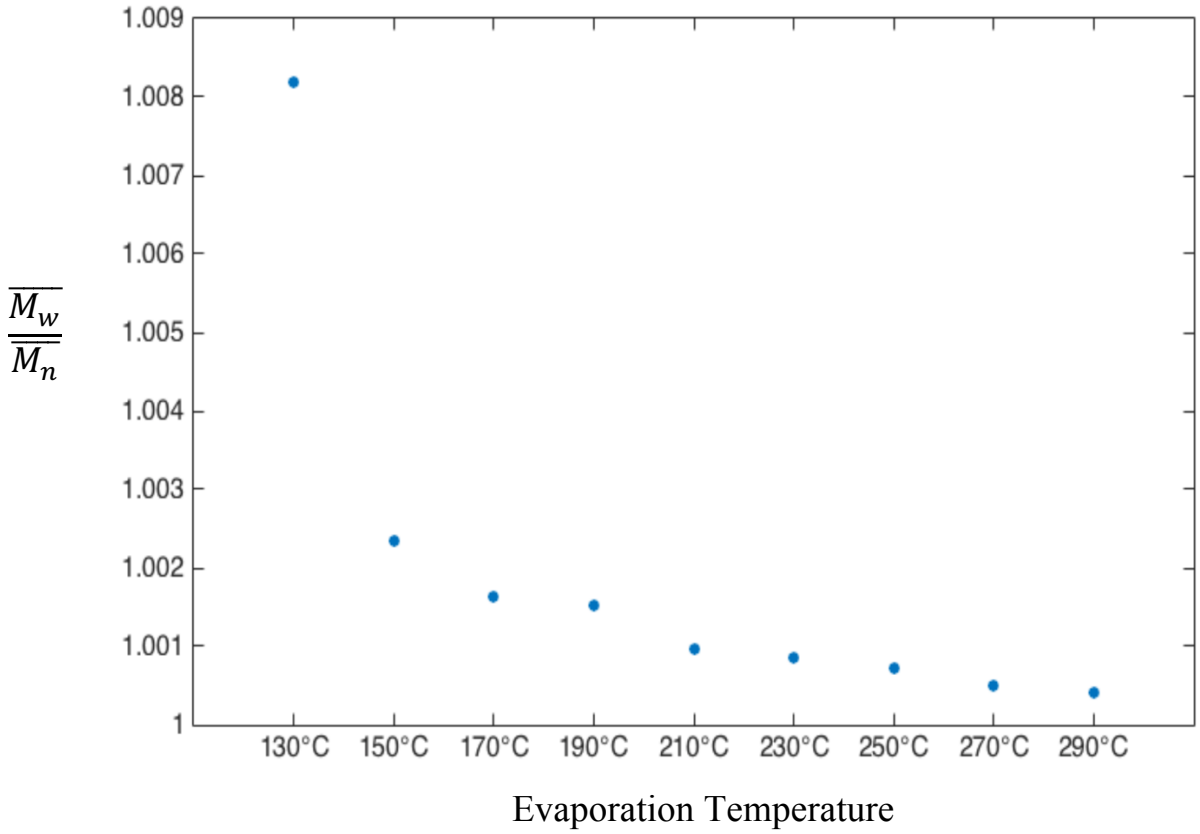

Figure 3.3.4: The relevant "$\overline{M_w}/\overline{M_n}$" of each separated polystyrene product calculated in Fig. 3.3.3.

polystyrene product (that from simulated results in Fig.3.3.3) ranges from 1.0004 to 1.0023, except that the polydispersity index $\overline{M_w}/\overline{M_n}$ of the first product is 1.0082, as shown in Fig. 3.3.4.

Furthermore, the polydispersity index can be successively improved by iterative purification. For example, we can use the product of the first purification obtained at 290 ℃ (product of 563 K in Fig.3.3.3) as the starting material to simulate the polydispersity index as a function of iteration time. The procedure of this simulation is the same as that of Fig.3.3.2. As shown in Fig.3.3.5 upon second iterative purification, the polydispersity index of the product deviates from 1 only on the order of a few ppm.

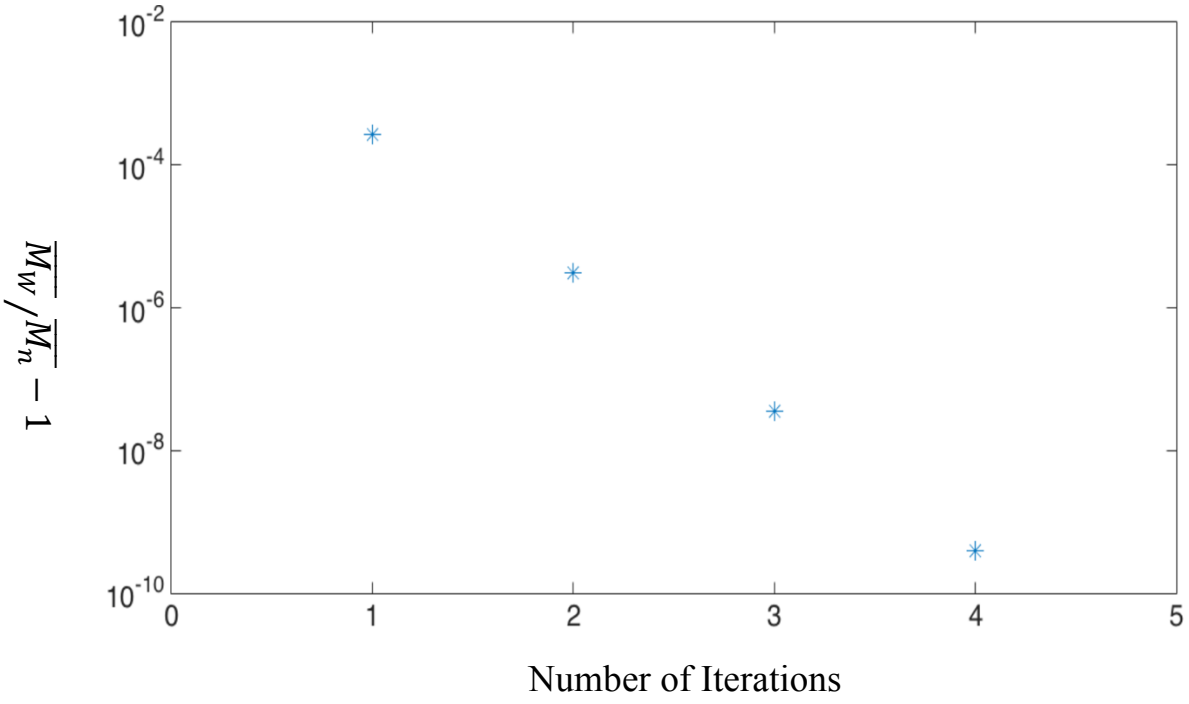

Figure 3.3.5: "$\overline{M_W}/\overline{M_n} - 1$" as a function of iteration times at 290℃.

3.4 Conclusion

In conclusion, calculated results show that vapor pressure of N-mer polystyrene with N ranging from 2 to 9 has a strong dependence on polymerization index and it is also very sensitive to the temperature. These calculated vapor pressures as functions of N and temperature will guide the experimental procedures as described in Chapter 4. The numerical simulation of polydispersity index predicts the evaporative purification technique has an excellent ability to separate a polydisperse sample into highly monodisperse components for N ranging from 1 to 9. The production of completely monodisperse polymer seems to be achievable upon the iterative purifications. In order to demonstrate the feasibility of the time range, we still need to test the real time scale of the evaporation via experiments.

4. Experimental studies of polystyrene purification by evaporation

4.1 Introduction

In this chapter, I will describe experimental work of evaporative purification for high quality polystyrene (with $\overline{M_w} = 600\ g/mol$ and $\overline{M_w} = 890\ g/mol$) and industrial grade polystyrene with $\overline{M_w} = 1200\ g/mol$. The purity of purified products, productivity of evaporative purification, molecular weight distribution of starting samples and upper limit of isolated N-mers are analyzed through experimental data of T_g values and evaporated masses. Finally, an alternative form of quantifying T_g from oligomer to polymer is proposed.

4.2 Evaporative purification of high quality polystyrene with $\overline{M_w} = 600g/mol$ and $\overline{M_w} = 890g/mol$

This technique has been experimentally tested for polystyrene samples with molecular weight distributions: $\overline{M_w} = 600\ g/mol$, $\overline{M_w}/\overline{M_n} = 1.2$; $\overline{M_w} = 890\ g/mol$, $\overline{M_w}/\overline{M_n} = 1.2$ both purchased from Polymer Source Inc. This experiment follows the same procedure used in the simulations of evaporation, as sketched in Fig. 4.2.1. The mass of each deposition product is recorded at equal

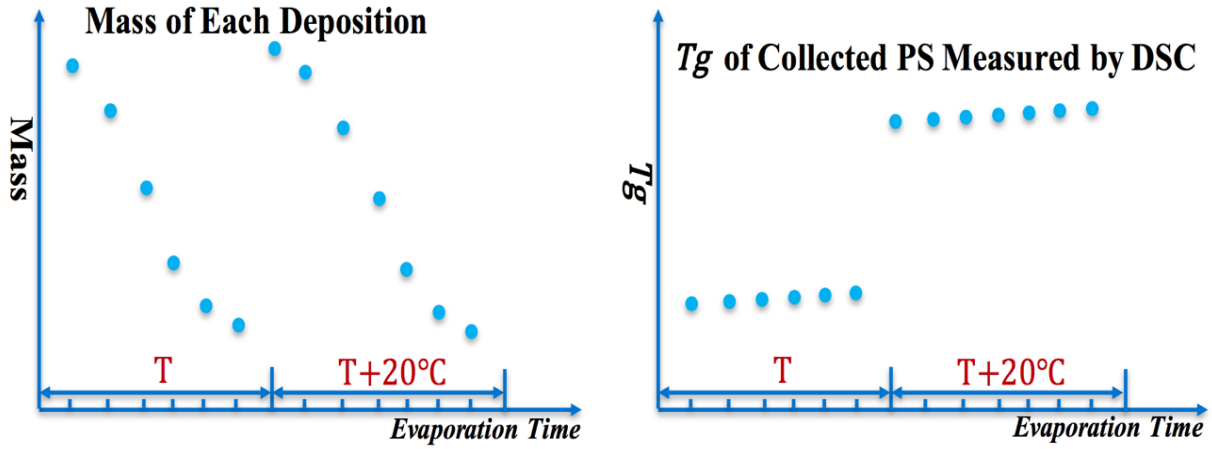

Figure 4.2.1: Schematic diagram showing the procedure for evaporative deposition of polystyrenes.

time intervals (120 minutes). Once the deposited mass reduces to less than 0.3 milligrams, the temperature is increased by 20 ℃. Following this process from low to high temperature ensures that at each temperature we are exhausting the smallest N value remaining in the sample. We keep doing this process until a sample temperature of 300 ℃. At temperatures greater than this, thermal decomposition of polystyrene has been shown to increase rapidly [43]. The deposited product at each time interval is then transferred to a sample pan and Differential Scanning Calorimeter (Q100 type of TA instruments) is performed with a heating/cooling rate of 10 K/min to measure the T_g. Fig. 4.2.2 shows the working temperature, the mass of product collected from each time interval and

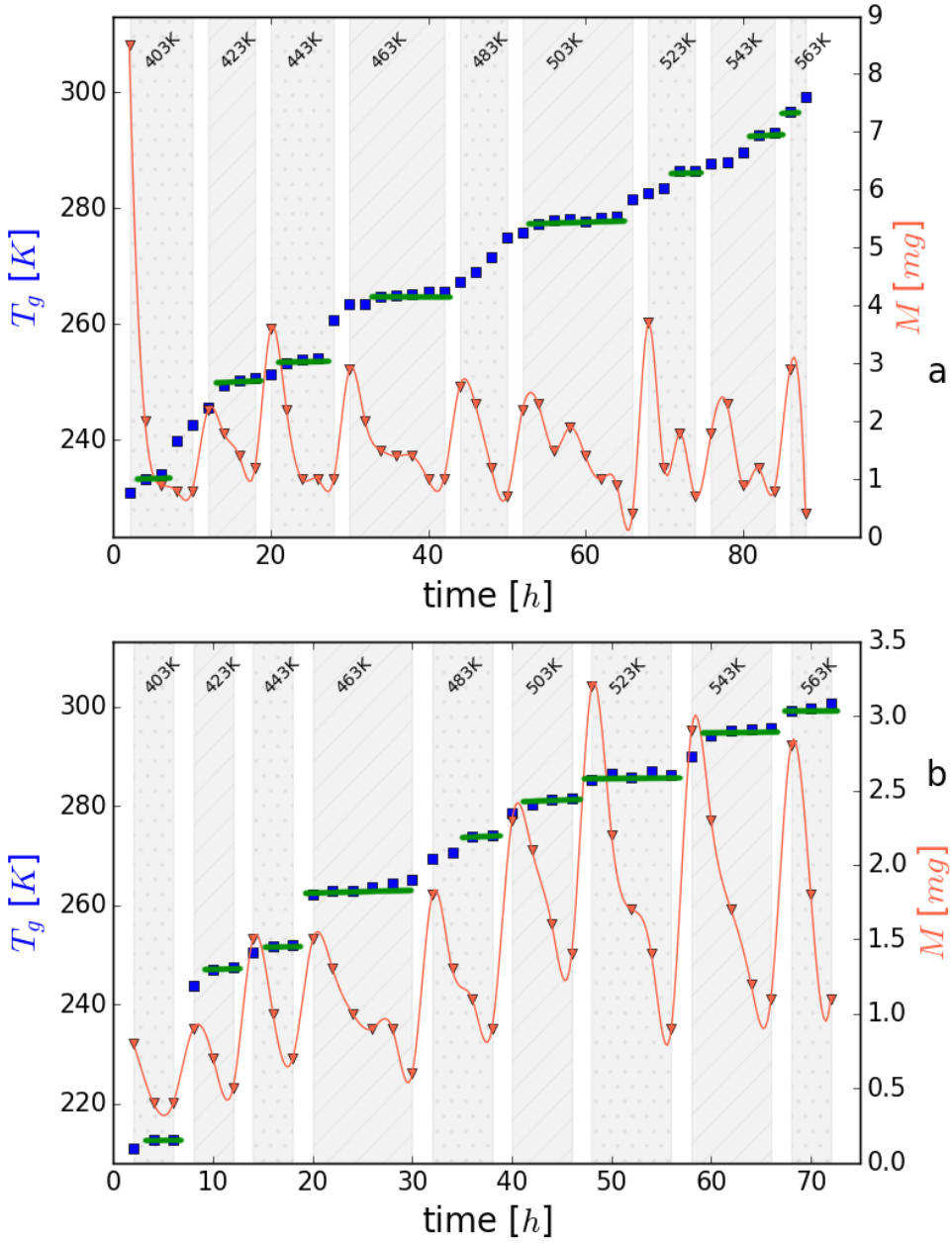

Figure 4.2.2: Deposited mass collected for each time interval and T_g values of those deposited components. The source samples are $\overline{M_w} = 600\ g/mol$ PS (top), $\overline{M_w} = 890\ g/mol$ PS (bottom). The deposited mass of each 2 hours is labelled as red triangle symbol. T_g values of isolated *N*-styrene are labelled as blue square symbols. T_g values exhibiting plateaus are marked by green lines.

the measured T_g for polystyrene with $\overline{M_w} = 600\ g/mol$ (top) and $\overline{M_w} = 890\ g/mol$ (bottom).

The composition of each product is time dependent, which results in a time dependent T_g. Suppose the majority of *N*-mer has already been deposited at temperature T, then the temperature is increased to $(T + 20)$ ℃ to deposit (*N*+1)-mer. The initial product may still contain some *N*-mer at this new temperature. If we continue to deposit at the same temperature, almost only (*N*+1)-mer will be collected for a long period, since the remaining *N*-mer has been totally evaporated off and the deposition rate of (*N*+2)-mer is significantly lower at this temperature. At this point, we should expect to observe the same T_g value of these products collected during this period and evidence for this is seen from the plateaus of T_g values in Fig. 4.2.2 marked by green lines. If we continue to deposit at this temperature, most of (*N*+1)-mer will have been exhausted and the evaporation rate of (*N*+1)-mer becomes comparable to that of (*N*+2)-mer due to the reduction in mole fraction of (*N*+1)-mer. Thus, appreciable amount of (*N*+2)-mer will start to be deposited. Comparing $\overline{M_w} = 600\ g/mol$ PS with $\overline{M_w} = 890\ g/mol$ PS, we find that almost the same *N*-mer is collected at the same deposition temperature. Only the evaporation at 483 K failed to produce a

defined plateau in the T_g value for $\overline{M_w} = 600\ g/mol$ PS. The reason may be that there is still a lot of *N*-mer remaining after the evaporation at 463 K and the difference of evaporation rates between *N*-mer and (*N*+1)-mer becomes less significant at 483 K. In order to optimize the time intervals of collecting pure *N*-mer component, one may use a quartz crystal microbalance (QCM) sensor to monitor the deposition rate.

The smallest N-mer associated with the first plateau of T_g at 403 K is evaluated as 3-mer based on the Fox-Flory relation as introduced in Section 1.5. Then N-mer separated at 423 K is considered as 4-mer. It is notable that this experiment is able to produce 9 plateaus of T_g which means 9 pure components associated with *N*=3~11 are isolated. The evaluated values of N may easily deviate from the actual values by 1, but unlikely by 2. The T_g values of these 9 components differ by 63 K. The monomer and dimer could also be easily isolated if a lower starting temperature is employed and time intervals of collecting are well optimized. High efficiency of collecting is achieved with both starting samples. The sample source of $\overline{M_w} = 600\ g/mol$ PS is 80.1 mg and 75.7 mg is evaporated, leaving 4.4 mg of materials with $N \geq 14$. 70.8 mg is collected out of the 75.7 mg for a 94% efficiency. However, the efficiency for collecting pure *N*-mer is only 50% based

on the mass of deposited materials exhibiting plateaus of T_g. Smaller N-mer remaining in the mixture will become waste at new evaporation temperature and it will continuously disable the production of plateaus of T_g values. Thus, the efficiency for collecting pure N-mers will be further improved, once time intervals of collecting pure N-mers are optimized or the number of plateaus is maximized by monitoring the precise deposition rate of each N-mer. We have tested our technique in a glove box full of nitrogen gas and it still worked quite

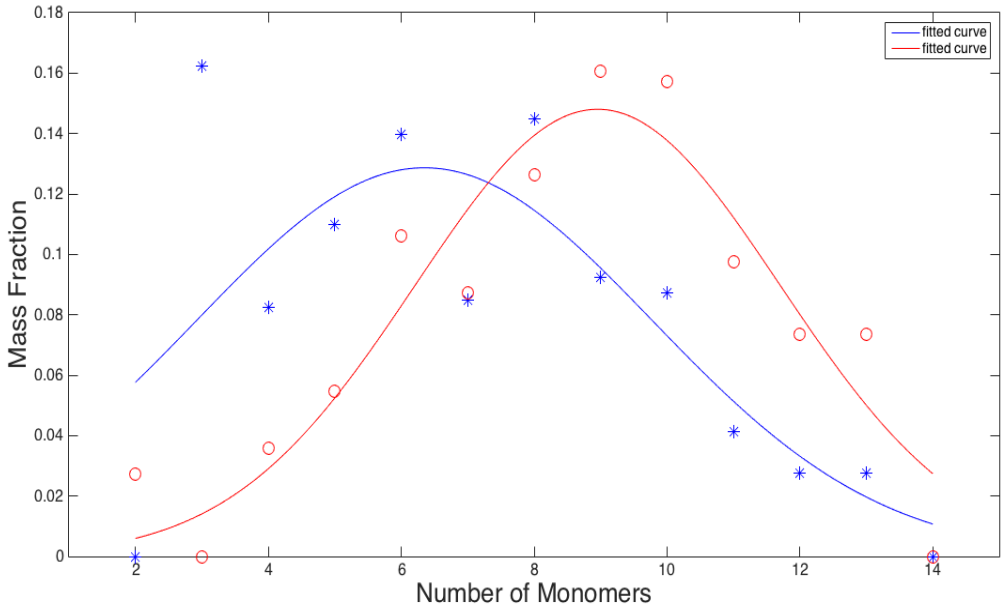

Figure 4.2.3: Mass distributions of evaporated components during the process of evaporation. The masses evaporated from the $\overline{M_w} = 600\ g/mol$ PS are labelled by the blue star symbols, and the masses evaporated from the $\overline{M_w} = 890\ g/mol$ PS are labelled by the red open circles. The fitting curves are based on Gaussian functional forms and are simply meant to guide the eye. The blue fitting curve is for the $\overline{M_w} = 600\ g/mol$ PS; the red fitting curve is for the $\overline{M_w} = 890\ g/mol$ PS.

well at atmospheric pressure, but at the cost of reduced efficiency of deposition. The evaporated masses can be used to estimate the molecular weight distributions of each polystyrene sample. As mentioned above, the composition of evaporated materials is time dependent. The first product at a particular temperature may contain an appreciable amount of (*N*-1)-mer, while the first product at next higher temperature may contain non-negligible amount of *N*-mer. We expect the amount of *N*-mer cancels out that of (*N*-1)-mer. If so, it will be a reasonable way to estimate the amount of *N*-mer by just considering the total mass evaporated at each temperature. Fig.4.2.3 shows the evaporated mass fraction at each temperature for $\overline{M_w} = 600\ g/mol$ and $\overline{M_w} = 890\ g/mol$ PS samples. The amount of unseparated monomer and dimer is not included in the two cases. $\overline{M_w}$, $\overline{M_n}$ and $\overline{M_w}/\overline{M_n}$ values are calculated based on this data for the two samples. For $\overline{M_w} = 600\ g/mol$ PS, I obtain the calculated values: $\overline{M_n} = 654.30\ g/mol$, $\overline{M_w} = 764.49\ g/mol$ and $\overline{M_w}/\overline{M_n} = 1.17$ which is slightly smaller than $\overline{M_w}/\overline{M_n} = 1.2$ quoted by the company. The probable reason is that all the evaporated material (still containing a significant amount of the monomer and dimer) at the starting temperature (130 ℃) is considered as 3-mers when we do the calculation. For $\overline{M_w} = 890\ g/mol$ PS, the calculated values is $\overline{M_n} =$

$849.13\ g/mol$, $\overline{M_w} = 957.44\ g/mol$ and $\overline{M_w}/\overline{M_n} = 1.1276$ which is quite consistent with $\overline{M_w}/\overline{M_n} = 1.12$ quoted by the company. The last separated component is denoted as N_{max}-mer. In these calculations, the remaining amount of larger *N*-mers is included and it is divided into equal amount of $(N_{max}+1)$-mer and $(N_{max}+2)$-mer, which is thought to be reasonable, because the measured T_g value of remaining materials is higher than the T_g value of any previously isolated component.

In conclusion, the evaporative purification has successfully separated the polystyrene samples with initial narrow molecular weight distributions into much more monodisperse components illustrated by plateaus of T_g. The following section will test whether this method will still work well for a much more polydisperse sample.

4.3 Evaporative purification of industrial grade polystyrene with $\overline{M_w} = 1200 g/mol$

This method has also been tested for the purification of $\overline{M_w} = 1200\ g/mol$ polystyrene with $\overline{M_w}/\overline{M_n} = 1.6$ purchased from Scientific Polymer Products. The price of this polymer is 45 USD per 500 g, which is 3 orders of magnitude less expensive than the polymers (150 USD/g) we used from Polymer Source.

Purification was carried out in a similar way to this sample, which also produced the plateaus of T_g values at each temperature as shown in Fig.4.3.1, suggesting that *N*-mer components with the same purity were separated from this industrial grade polymer. The largest difference that occurred by changing the source of starting polymer is that the *N*-mer separated at a particular temperature is not the same as that of $\overline{M_w} = 600\ g/mol$ PS and $\overline{M_w} = 890\ g/mol$ PS. This is likely a result of the fact that this $\overline{M_w} = 1200\ g/mol$ PS prepared by free radical polym-

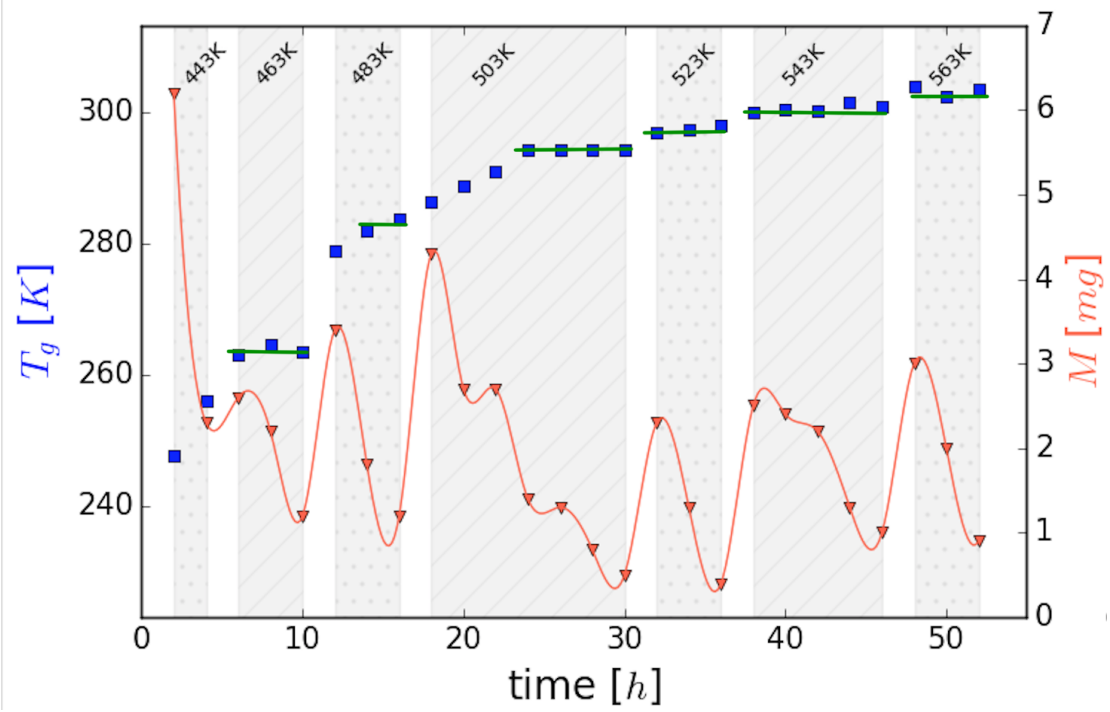

Figure 4.3.1: Measured deposited mass and T_g values of evaporatively isolated components of *N*-styrene for $\overline{M_w} = 1200\ g/mol$ polystyrene sample. The deposited mass of each 2 hours is labelled as red triangle symbol. T_g values of isolated *N*-styrene are labelled as blue square symbols. T_g values exhibiting plateaus are marked by green lines.

erization contains different chain ends than the $\overline{M_w} = 600\ g/mol$ PS and $\overline{M_w} = 890\ g/mol$ PS prepared by anionic polymerization.

The eventual N-mer separated at the highest experimental temperature also varies with different types of polystyrenes. The upper limit of the isolated N-mer will be discussed below as well as the comparison of T_g values for separated N-mers.

4.4 Discussion

4.4.1 T_g values of separated components

As discussed in Section 4.2, each plateau of T_g value corresponds to a particular *N*-mer. We plot the T_g values measured in each of the plateaus as a function of polymerization index *N* as well as the T_g values of the initial three samples, as shown in Fig. 4.4.1. We find the T_g values of the separated components are nearly overlapped at each polymerization index, which suggests that the same N-mers are isolated in each case. The T_g values are the same and are independent of the starting samples, which is a proof that these separated components are nearly pure N-mers. These results also predict the practical upper limit of the largest N value that can be isolated by this evaporative purification. As mentioned above, the temperature is upper limited to avoid thermal decomposition. Since polystyrene is known to degrade at temperatures greater than 573 K [44], the highest tempera-

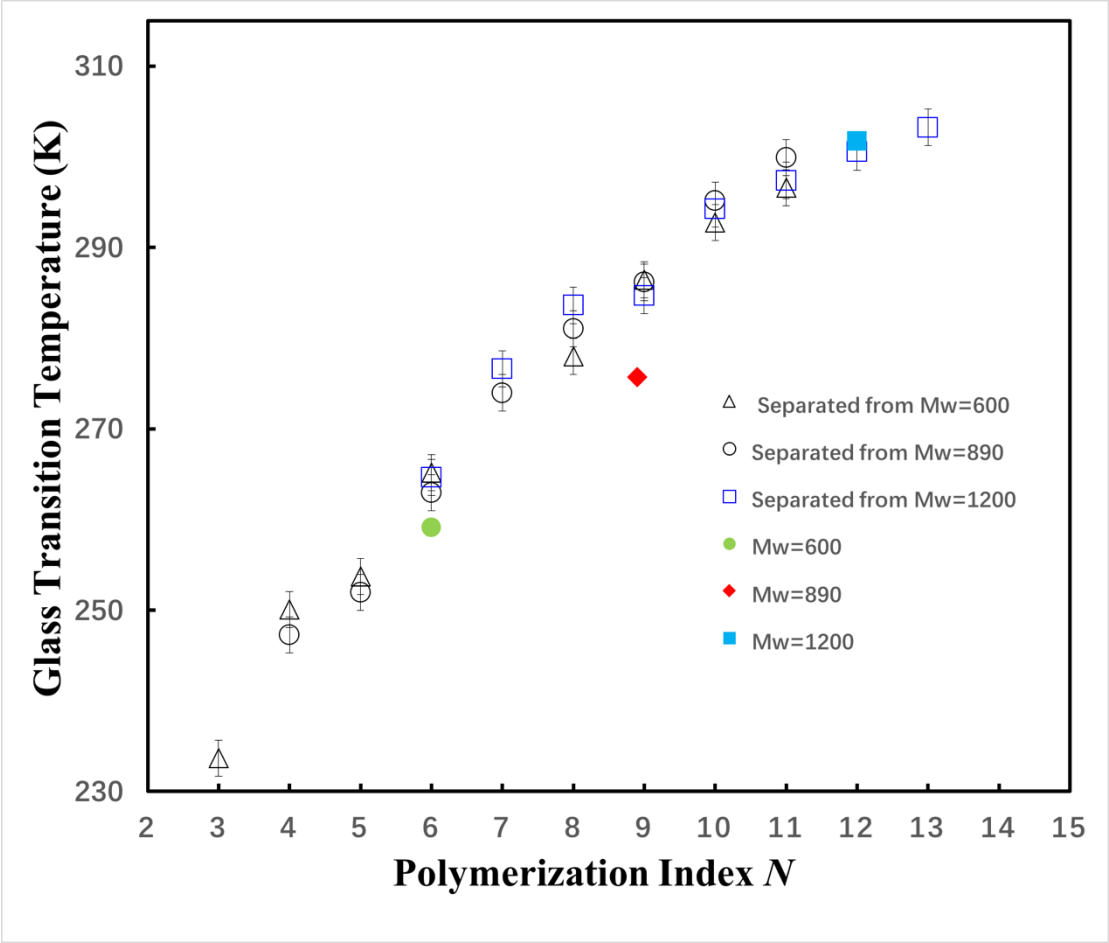

Figure 4.4.1: T_g values of *N*-styrene as isolated from the 3 different initial polydisperse polystyrenes, as well as the T_g values of the initial polydisperse samples. T_g values of $\overline{M_w} = 600\ g/mol$, $\overline{M_w} = 890\ g/mol$, and $\overline{M_w} = 1200\ g/mol$ initial polydisperse polystyrenes are labelled as green circle symbol, red square symbol and blue square symbol, respectively. T_g values of *N*-styrene isolated from $\overline{M_w} = 600\ g/mol$, $\overline{M_w} = 890\ g/mol$, and $\overline{M_w} = 1200\ g/mol$ polystyrenes are labelled as open triangle symbols, open circle symbols and open square symbols, respectively. The polymerization index *N* of each isolated styrene is estimated by Fox-Flory relation as introduced in section 1.5. T_g values of isolated *N*-styrene are from T_g values exhibiting plateaus in Fig. 4.2.2 and Fig. 4.3.1.

ture used is 563 K so far and the largest deposited *N* value at this temperature is

13 at a maximum rate of about 1 mg/hour. If we continue to deposit at this temperature, the 13-mer can be eventually exhausted and the 14-mer will be deposited, but it will take a much longer time due to the approximated 2 orders of magnitude lower deposition rate based on the simulation. It seems that the upper bound of *N* value that can be isolated in reasonable quantities within reasonable time will be 13 for the case of polystyrene. However, the polydispersity of the remaining material with $N \geq 14$ can be significantly reduced after the entire process of isolating pure *N*-mers for $N \leq 13$.

4.4.2 Quantification of T_g from oligomer to polymer

These separated pure *N*-mers provide an opportunity to precisely investigate the T_g of oligomers (polymers with relatively low polymerization index) with single molecular weight. The T_g values shown in Fig.4.4.1 can be used to test the Fox-Flory relationship [3], and the polymer chain ends have a strong impact on the T_g values of these oligomers, which has been demonstrated in previous studies [9,45]. We develop an alternative form to quantify the T_g from oligomer to polymer by combining the Fox relation and the effects of chain ends on the glass transition temperature. The Fox relation for the glass transition temperature of a

miscible mixture containing two components, with weight fractions w_1, w_2 and T_g values T_g^1 and T_g^2 is written as:

$$\frac{1}{T_g} = \frac{w_1}{T_g^1} + \frac{w_2}{T_g^2}. \tag{4.4.1}$$

In analogy to this case, we consider one polymer chain consisting of two components: chain segments and chain ends. If the weight fraction of the chain ends is $\frac{1}{\beta N}$, the weight fraction of the chain segments is $\left(1 - \frac{1}{\beta N}\right)$, where the parameter β is a result of the fact that there are two chain ends and that the weight fraction depends on the relative size of chain ends and chain segments. The glass transition is traditionally discussed in terms of volume, and volume fraction may be a more reasonable choice. This difference is absorbed into the β value which relates the weight fraction of the chain end groups. Motivated by the similar procedure with free volume arguments used to derive Eq. (7) in Ref. [46], we consider the T_g value of chain segments as T_g^∞ and the T_g value of chain ends as T_g^0. Then we can substitute them into Eq. (4.4.1) to get:

$$\frac{1}{T_g(N)} = \frac{1/(\beta N)}{T_g^0} + \frac{1 - 1/(\beta N)}{T_g^\infty}. \tag{4.4.2}$$

This can be further written as:

$$T_g(N) = \frac{T_g^{\infty} T_g^0}{\frac{1}{\beta N} T_g^{\infty} + \left(1 - \frac{1}{\beta N}\right) T_g^0} = \frac{T_g^{\infty}}{1 + \frac{1}{\beta N}\left(\frac{T_g^{\infty}}{T_g^0} - 1\right)}. \quad (4.4.3)$$

Let $x = \frac{1}{N}$ and $A = \frac{1}{\beta}\left(\frac{T_g^{\infty}}{T_g^0} - 1\right)$; then the $T_g(N)$ can be expressed as:

$$T_g(N) = f(x) = \frac{T_g^{\infty}}{1 + Ax}. \quad (4.4.4)$$

The Taylor expansion of $f(x)$ at $x = 0$ (for $N \gg 1$) is:

$$f(x) = f(0) + f^{(1)}(0)x + \cdots \cong T_g^{\infty}(1 - Ax). \quad (4.4.5)$$

It is interesting to find that in the case of $N \gg 1$, the first order in $1/N$ of this equation recovers the Fox-Flory relationship $T_g(N) \cong T_g^{\infty}(1 - A/N)$, where $A = \frac{1}{\beta}\left(\frac{T_g^{\infty}}{T_g^0} - 1\right)$. In the case where *N* is not large, we choose the full Eq. (4.4.3) to fit T_g values only by adjusting the physical parameters in A. To make the comparison, we use the T_g values from Fig. 4.4.1 for the *N*-mers separated from $\overline{M_w} = 890\ g/mol$ polystyrene prepared by anionic polymerization and those for more polydisperse polystyrenes with much higher molecular weight in Ref. [47] (These higher $\overline{M_w}$ polystyrenes are made by the same way and T_g values are measured by the same instrument and procedures as described above).

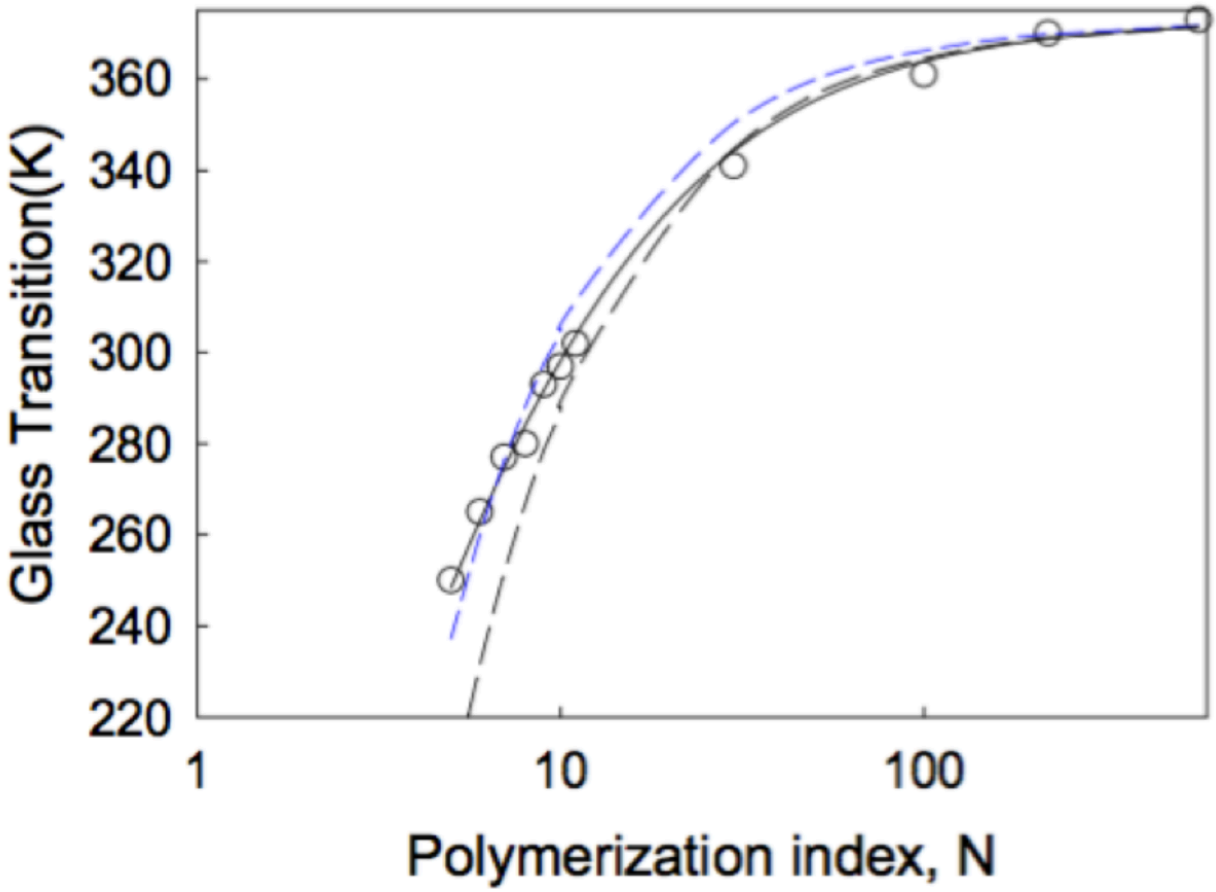

Figure 4.4.2: T_g values of *N*-styrene ($N \leq 11$), and more polydisperse ($N > 11$) polystyrene and fits to Eq. (4.4.3) as well as Fox-Flory expressions. These *N*-styrenes are from the $\overline{M_w} = 890\ g/mol$ PS as described in this experiment; while these more polydisperse polystyrenes are the same type as the *N*-styrenes.

The fitting results are shown in Fig. 4.4.2, where the solid line is the fit to Eq. (4.4.3), and the dashed lines are best fit to the common Fox-Flory relationship(blue), and the Fox-Flory relationship with parameters usually employed for larger N (black). It is evident that our functional form has a better fit over the entire range N (from $N \sim 5$ to $N \to \infty$).

5. Concluding remarks and future work

In summary, I have described and developed a simple technique to separate polydisperse polystyrenes into pure components from 3-mers to 13-mers which have the highest degree of monodispersity as yet reported. This technique can even produce the same quality of N-mers from low-cost samples with an initial $\overline{M_w}/\overline{M_n}$ of 1.6 as those produced from the expensive polymers with narrower molecular weight distributions. Based on the T_g values of these pure components, the Fox equation for the T_g of mixtures is developed into a simple relation which is able to accurately quantify the T_g values from oligomer to polymer.

The upper bound of N-mer isolated by this evaporative purification technique is limited by the eventual thermal decomposition temperature, which restricts the production of completely monodisperse polymers with high molecular weight. Quantities of isolated pure components by this technique in our lab are also limited at milligram level. The evaporative purification requires nothing but clean vacuum and temperature control, which is readily scalable to produce larger quantities of pure materials. However, many challenges still exist in the engineering of scalability. For example, how to keep distinct temperature difference between large-area top collector or condenser and the evaporator stage in a short

distance, and how to minimize temperature gradients on the large surface of heating stage as well as those vertical to the surface.

For future applications, pure materials separated by this technique could in turn be used experimentally to determine the actual vapor pressures of the *N*-mers. These separated pure *N*-mers are ideal specimens to precisely study the physical properties depended on molecular weight, such as T_g, solubility, properties of crystallization, and phase separations. This technique has been shown to successfully separate the synthetic polystyrene into *N*-mers and will be applied to other polymers systems, such as poly(ethylene glycol) (PEG). The completely monodisperse PEG provides perspectives to achieve detailed insight into the precise correlation between the monomer sequence and biological system, which might contribute to the design of functional materials for important biomedical applications, such as gene and drug delivery, tissue-repair scaffolds and clinical sensors.

Reference

[1] Strobl, G. R. (1997). *The physics of polymers* (Vol. 2). Berlin: Springer.

[2] Rogošić, M., Mencer, H. J., & Gomzi, Z. (1996). Polydispersity index and molecular weight distributions of polymers. *European polymer journal*, *32*(11), 1337-1344.

[3] Fox Jr, T. G., & Flory, P. J. (1950). Second-order transition temperatures and related properties of polystyrene. I. Influence of molecular weight. *Journal of Applied Physics*, *21*(6), 581-591.

[4] V. Marcon and N. F. A. van der Vegt, *Soft Matter* 10, 9059 (2014).

[5] D. J. Plazek and V. M. O'Rourke, *J. Polym. Sci.* 9, 209 (1971).

[6] S.S. Patil, S.K. Menon, P.P. Wadgaonkar, *Polym. Int.* 64 413-420 (2014).

[7] Hartmann, L., & Börner, H. G. (2009). Precision Polymers: Monodisperse, Monomer-Sequence-Defined Segments to Target Future Demands of Polymers in Medicine. *Advanced Materials*, *21*(32-33), 3425-3431.

[8] Sugiyama, K., Hirao, A., Hsu, J. C., Tung, Y. C., & Chen, W. C. (2009). Living Anionic Polymerization of Styrene Derivatives para-Substituted with π-Conjugated Oligo (fluorene) Moieties. *Macromolecules*, *42*(12), 4053-4062.

[9] Hatakeyama, T., & Serizawa, M. (1982). Glass transition of oligostyrene with different end groups. *Polymer Journal*, *14*(1), 51-57.

[10] Li, S. J., Xie, S. J., Li, Y. C., Qian, H. J., & Lu, Z. Y. (2016). Influence of molecular-weight polydispersity on the glass transition of polymers. *Physical Review E*, *93*(1), 012613.

[11] Beardsley, T. M., & Matsen, M. W. (2016). Universality between Experiment and Simulation of a Diblock Copolymer Melt. *Physical Review Letters*, *117*(21), 217801.

[12] Ueberreiter, K., & Kanig, G. (1952). Self-plasticization of polymers. *Journal of Colloid Science, 7*(6), 569-583.

[13] Fujishige, S., & Ohguri, N. (1975). Chromatographic fractionation of styrene oligomer and 1H-NMR spectra of pure styrene n-mers. *Macromolecular Chemistry and Physics*, *176*(1), 233-237.

[14] Kottisch, V., Gentekos, D. T., & Fors, B. P. (2016). "Shaping" the Future of Molecular Weight Distributions in Anionic Polymerization. *ACS Macro Letters*, *5*(7), 796-800.

[15] Sweat, D. P., Kim, M., Schmitt, A. K., Perroni, D. V., Fry, C. G., Mahanthappa, M. K., & Gopalan, P. (2014). Phase Behavior of Poly (4-hydroxystyrene-block-styrene) Synthesized by Living Anionic Polymerization of an Acetal Protected Monomer. *Macromolecules*, *47*(18), 6302-6310.

[16] Taylor, F. S. (1945). The evolution of the still. *Annals of science*, *5*(3), 185-202.

[17] Houghton, P. J., & Raman, A. (1998). Chromatographic fractionation procedures. In *Laboratory Handbook for the Fractionation of Natural Extracts* (pp. 66-81). Springer US.

[18] Lattimer, R. P., Harmon, D. J., & Welch, K. R. (1979). Characterization of low molecular weight polymers by liquid chromatography and field desorption mass spectroscopy. *Analytical Chemistry*, *51*(8), 1293-1296.

[19] Takahashi, K., Matsuyama, S., Kinugasa, S., Ehara, K., Sakurai, H., Horikawa, Y., ... & Bounoshita, M. (2014). Molecularly uniform poly (ethylene glycol) certified reference material. *Metrologia*, *52*(1), 8.

[20] Chickos, J. S., & Hanshaw, W. (2004). Vapor pressures and vaporization enthalpies of the n-alkanes from C21 to C30 at T= 298.15 K by correlation gas chromatography. *Journal of Chemical & Engineering Data*, *49*(1), 77-85.

[21] Bawn, C. E. H., Freeman, R. F. J., & Kamaliddin, A. R. (1950). High polymer solutions. Part I-Vapour pressure of polystyrene solutions. *Transactions of the Faraday Society*, *46*, 677-684.

[22] Sakurada, I., Nakajima, A., & Fujiwara, H. (1959). Vapor pressures of polymer solutions. II. Vapor pressure of the poly(vinyl alcohol)-water system. *Journal of Polymer Science Part A: Polymer Chemistry*, *35*(129), 497-505.

[23] Sanchez, I. C., & Lacombe, R. H. (1976). An elementary molecular theory of classical fluids. Pure fluids. *The Journal of Physical Chemistry*, *80*(21), 2352-2362.

[24] "Lecture 23: 12.05.05 Lattice Models of Materials; Modeling Polymer Solution", 2005, *MIT OpenCourseWare*, Foundamentals of Materials Science.

[25] Flory, P. J. (1942). Thermodynamics of high polymer solutions. *The Journal of chemical physics*, *10*(1), 51-61.

[26] Nemirovsky, A. M., Bawendi, M. G., & Freed, K. F. (1987). Lattice models of polymer solutions: Monomers occupying several lattice sites. *The Journal of chemical physics*, *87*(12), 7272-7284.

[27] E.A. Guggenheim, Proc. R. SOC. London, *Ser.* A, 183,203 (1944)**.**

[28] E.A. Guggenheim, "Mixtures", Oxford University Press, London, 1952, Chapters X and XI.

[29] E.A. Guggenheim, "Application of Statistical Mechanics", Oxford University Press, London, 1966, Chapters 4 and 7.

[30] Sanchez, I. C., & Lacombe, R. H. (1978). Statistical thermodynamics of polymer solutions. *Macromolecules*, *11*(6), 1145-1156.

[31] Rodgers, P. A. (1993). Pressure–volume–temperature relationships for polymeric liquids: a review of equations of state and their characteristic parameters for 56 polymers. *Journal of Applied Polymer Science*, *48*(6), 1061-1080.

[32] ISO 11357-2: Plastics-Differential scanning calorimetry-Part 2: Determination of glass transition temperature (1999).

[33] Debenedetti, P. G., & Stillinger, F. H. (2001). Supercooled liquids and the glass transition. *Nature*, *410*(6825), 259.

[34] Ehrenfest, P. *Commun. Kamerlingh Onnes Lab., Leiden Suppl.* 1933, 75b.

[35] Simons, B. (1997). Phase transitions and collective phenomena. *Lecture Notes, available at http://www. tcm. phy. cam. ac. uk/~ bds10/phase. html*.

[36] Segre, P. N., Prasad, V., Schofield, A. B., & Weitz, D. A. (2001). Glasslike kinetic arrest at the colloidal-gelation transition. *Physical Review Letters*, *86*(26), 6042.

[37] Bernabei, M., Moreno, A. J., & Colmenero, J. (2008). Dynamic arrest in polymer melts: Competition between packing and intramolecular barriers. *Physical review letters*, *101*(25), 255701.

[38] K. C. D. Hickman. (1944). High-vacuum short path distillation-a review. *Chem. Rev. 34,* 51.

[39] Richardson, M. J., & Savill, N. G. (1975). Derivation of accurate glass transition temperature by differential scanning calorimetry. *Polymer*, *16*(10), 753-757.

[40] Langmuir, I. (1913). The vapor pressure of metallic tungsten. *Physical review*, *2*(5), 329.

[41] Takahashi, Y., Matsuzaki, K., Iijima, M., Fukada, E., Tsukahara, S., Murakami, Y., & Maesono, A. (1993). Determination of evaporation rate and vapor pressure of organic monomers used for vapor deposition polymerization. *Japanese journal of applied physics*, *32*(6B), L875.

[42] K. J. Laidler and J. H. Maiser, *Physical Chemistry* (Benjamin Cummings, San Francisco, 1982), p 180.

[43] Malhotra, S. L., Hesse, J., & Blanchard, L. P. (1975). Thermal decomposition of polystyrene. *Polymer*, *16*(2), 81-93.

[44] Guaita, M. (1986). Thermal degradation of polystyrene. *Polymer International*, *18*(4), 226-230.

[45] Zhang, L., Marsiglio, J. A., Lan, T., & Torkelson, J. M. (2016). Dramatic Tunability of the Glass Transition Temperature and Fragility of Low Molecular Weight Polystyrene by Initiator Fragments Located at Chain Ends. *Macromolecules*, *49*(6), 2387-2398.

[46] Fox, T. G., & Loshaek, S. (1955). Influence of molecular weight and degree of crosslinking on the specific volume and glass temperature of polymers. *Journal of Polymer Science*, *15*(80), 371-390.

[47] Qi, D., Daley, C. R., Chai, Y., & Forrest, J. A. (2013). Molecular weight dependence of near surface dynamical mechanical properties of polymers. *Soft Matter*, *9*(37), 8958-8964.

Appendix: published papers

Zhu, S., Chai, Y., & Forrest, J. A. (2017). Evaporative purification to produce highly monodisperse polymers: Application to polystyrene for n= 3–13 and quantification of T_g from oligomer to polymer. *Physical Review Materials, 1*(2), 025605.